King's Research Portal

[Link to publication record in King's Research Portal](#)

Citation for published version (APA):
Mitzelfelt, K. A., Limphong, P., Choi, M. J., Kondrat, F. D. L., Lai, S., Kolander, K. D., Kwok, W.-M., Dai, Q., Grzybowski, M. N., Zhang, H., Taylor, G. M., Lui, Q., Thao, M. T., Hudson, J. A., Barresi, R., Bushby, K., Jungbluth, H., Wraige, E., Geurts, A. M., ... Benjamin, I. J. (2016). Human 343delT HSPB5 Chaperone associated with Early-onset Skeletal Myopathy causes Defects in Protein Solubility. *Journal of Biological Chemistry*. Advance online publication. https://doi.org/10.1074/jbc.M116.730481

Human 343delT HSPB5 Chaperone associated with Early-onset Skeletal Myopathy causes Defects in Protein Solubility*

Katie A. Mitzelfelt[1], Pattraranee Limphong[2], Melinda J. Choi[3], Frances D.L. Kondrat[4], Shuping Lai[3], Kurt D. Kolander[3], Wai-Meng Kwok[5], Qiang Dai[3], Michael N. Grzybowski[3], Huali Zhang[6], Graydon M. Taylor[7], Qiang Lui[7], Mai T. Thao[3], Judith A. Hudson[8], Rita Barresi[9], Kate Bushby[10], Heinz Jungbluth[11-13], Elizabeth Wraige[11], Aron M. Geurts[3], Justin L.P. Benesch[4], Michael Riedel[14], Elisabeth S. Christians[15], Alex C. Minella[16], Ivor J. Benjamin[1,3+]

[1]Department of Biochemistry, University of Utah, Salt Lake City, UT 84112, USA
[2]Arcturus Therapeutics, San Diego, CA 92121, USA
[3]Cardiovascular Center, Medical College of Wisconsin, Milwaukee, WI 53226, USA
[4]Department of Chemistry, University of Oxford, Oxford, UK
[5]Department of Anesthesiology and Department of Pharmacology&Toxicology, Medical College of Wisconsin, Milwaukee, WI 53226, USA
[6]Department of Pathophysiology, Xiangya School of Medicine, Central South University, Changsha City, Hunan 410078, China
[7]Division of Cardiology, Department of Medicine, University of Utah, Salt Lake City, UT 84132, USA
[8]Northern Genetics Service, Newcastle upon Tyne Hospitals NHS Foundation Trust, Newcastle upon Tyne, UK
[9]NHS England HSS for Rare Neuromuscular Diseases, Muscle Immunoanalysis Unit, Dental Hospital, Richardson Road, Newcastle upon Tyne, UK NE2 4AZ
[10]Neuromuscular Genetics, Newcastle University John Walton Centre for Muscular Dystrophy Research, MRC Centre for Neuromuscular Diseases, Institute of Genetic Medicine, International Centre for Life, Newcastle upon Tyne, UK NE1 3BZ
[11]Department of Paediatric Neurology, Neuromuscular Service Evelina Children's Hospital, Guy's & St Thomas' NHS Foundation Trust, London, UK, [12]Randall Division of Cell and Molecular Biophysics, Muscle Signalling Section, King's College London, UK, and [13]Department of Basic and Clinical Neuroscience Institute of Psychiatry, Psychology and Neuroscience (IoPPN), King's College London, UK
[14]PharmaCell, Maastricht, Netherlands
[15]Observatoire oocéanologique de Villefranche sur mer (UMR7009, UPMC/CNRS), Sorbonne Universités (Paris VI), Paris, France
[16]Blood Research Institute, BloodCenter of Wisconsin, Milwaukee, WI 53226, USA

+To whom correspondence may be addressed: Dr. Ivor J. Benjamin, Cardiovascular Center, Medical College of Wisconsin, 8701 Watertown Plank Road, Milwaukee, WI 53226, Telephone: (414) 955-6780, FAX: (414) 456-6515, Email: ibenjamin@mcw.edu

ABSTRACT

Mutations of HSPB5 (also known as CRYAB or αB-crystallin), a *bona fide* heat shock protein and molecular chaperone encoded by the *HSPB5 (crystallin, alpha B)* gene, are linked to various multisystem disorders featuring variable combinations of cataracts, cardiomyopathy, and skeletal myopathy. This study aims at investigating the pathological mechanisms involved in an early onset myofibrillar myopathy manifesting in a child harboring a homozygous recessive mutation in *HSPB5*, 343delT. To study HSPB5 343delT protein dynamics, we utilize model cell culture systems including induced pluripotent stem cells (iPSCs) derived from the 343delT patient (343delT/343delT) along with isogenic, heterozygous, gene-corrected control cells (WT KI/343delT), and BHK21 cells, a cell line lacking endogenous HSPB5 expression. 343delT/343delT and WT KI/343delT iPSC-derived skeletal myotubes (iSKMs) and cardiomyocytes (iCMs) did not express detectable levels of 343delT protein, contributable to extreme insolubility of the mutant protein. Overexpression

of HSPB5 343delT resulted in insoluble mutant protein aggregates and induction of a cellular stress response. Co-expression of 343delT with WT prevented visible aggregation of 343delT and improved its solubility. Additionally, *in vitro* refolding of 343delT in the presence of WT rescued its solubility. We demonstrate an interaction between WT and 343delT both *in vitro* and within cells. These data support a loss of function model for the myopathy observed in the patient, as the insoluble mutant would be unavailable to perform normal functions of HSPB5, though additional gain-of-function effects of the mutant protein cannot be excluded. Additionally, our data highlights the solubilization of 343delT by WT, concordant with the recessive inheritance of the disease and absence of symptoms in carrier individuals.

HSPB5 (also known as CRYAB or αB-crystallin) is a small molecular weight heat shock protein (sHSP)[#] encoded by the *HSPB5* gene and functions as a molecular chaperone. Its promoter contains a heat shock element (HSE), a stress-responsive binding site of heat shock transcription factor 1 (HSF1), which functionally upregulates the expression of *HSPB5*. Increased levels of HSPB5 can then go on to provide distinct cytoprotective effects engaged in restoring cellular homeostasis (reviewed in (1,2)). Additionally, *HSPB5* contains tissue-specific enhancer elements in its promoter that allow constitutive, high expression in the lens, heart, and skeletal muscle (3,4).

As a member of the sHSP family, HSPB5 contains a well-conserved central "α-crystallin" domain (ACD), flanked by N- and C-terminal regions (5). The ACDs dimerize, and assemble to form a polydisperse ensemble of oligomers, largely through dynamic interactions mediated by the terminal regions (6). The isolated ACD has been shown to have potent chaperone activity *in vitro* (7), and it is hypothesized that it might become exposed within the context of the wild-type protein in a manner regulated by phosphorylation (8) or cellular stress directly (9). The HSPB5 ACD contains two hydrophobic grooves, one between the β4 and β8 strands, and the other at the dimer interface, both of which

serve as putative binding sites for chaperone action (10). In addition, evidence also points at the involvement of the N-terminus in target binding (11). As such, current data suggests HSPB5 is a dynamic protein that is flexible in how it interacts with its diverse range of clients.

In striated muscle, HSPB5 acts as a chaperone for important structural client proteins including desmin (12-14), titin (15-18), and actin (14,19), a property that becomes particularly important under conditions of pathology or stress. *HSPB5/HSPB2* double knockout (DKO) mice exhibit progressive skeletal myopathy throughout life (20) with impact on cardiac muscle only observed under conditions of exogenous stress (21,22). More recently, a requirement for HSPB5 in muscle homeostasis has been demonstrated via modulation of argonaute 2 activity (23). DKO mice show reduced basal levels of skeletal muscle progenitor cells, or satellite cells, and defective muscle regeneration with cellular injury (23).

Multiple mutations in *HSPB5* are linked to human pathologies affecting the lens, heart, skeletal muscle, or some combination thereof with the underlying disease mechanism(s) only partially understood (reviewed in (24,25)). These mutations are either dominant or recessive and have variable penetrance and expressivity. Of the known mutations in *HSPB5* linked with (cardio-) myopathy, all but one result in aberrant protein aggregation of the mutant protein (reviewed in (25)). For the well-studied R120G mutation in HSPB5, the aggregates are thought to sequester other metastable proteins such as desmin (26-28). The relative contribution of loss versus gain-of-toxic function effects remain unclear for specific mutations.

An enhanced understanding of HSPB5 as a chaperone is needed to inform therapy development. Herein, we have investigated a recessive mutation in *HSPB5*, 343delT, found in a patient who presented at age four months with profound muscle stiffness, persistent creatine kinase elevation, and histopathological features of a myofibrillar myopathy (29). This homozygous recessive, single base deletion results in a frameshift and formation of a premature stop codon following addition of 14 missense residues (S115fs129X). The truncated protein is predicted to contain residues 1-115, having lost the C-

terminal extension, as well as a significant portion of the ACD. The patient's skeletal muscle biopsy shows dense, irregular staining of HSPB5, detectable only by an antibody recognizing the N-terminus of HSPB5 (NT-HSPB5). This band runs at the predicted molecular weight of 15 kDa on a western blot, smaller than the 22 kDa wildtype HSPB5 (WT) protein (29). Additionally, the biopsy shows intense, irregular staining of desmin and myotilin. At presentation, the patient exhibited neither signs of an associated cardiomyopathy nor cataracts, though with age, these symptoms may develop. Of note, the non-consanguineous parents, each heterozygous for 343delT, have no known symptoms attributed to this mutation, however, potential development of late-onset symptoms cannot be excluded.

To understand 343delT protein dynamics and their contribution to disease, we have incorporated the use of induced pluripotent stem cells (iPSCs) (30) derived from the patient as a unique system to permit study of endogenous 343delT protein within cell types of interest. Additionally, we used systems of overexpression in a cell line that lacks endogenous HSPB5 expression (reviewed in (31)), due to the recessive nature of the mutation, as well as *in vitro* analysis of 343delT. Herein we describe our findings that provide insights into molecular defects of 343delT in disease pathogenesis.

RESULTS

Generation of iPSCs for Investigation of 343delT— Fig. 1A shows the family pedigree of the patient harboring the homozygous, recessive 343delT mutation. Non-consanguineous parents are each heterozygous for the mutation and are asymptomatic, while the homozygous 343delT patient exhibits a severe, infantile-onset myopathy (29). To examine effects of 343delT (strategy outlined in Fig. 1B), we generated iPSCs from the patient's dermal fibroblasts through four factor reprogramming. Isogenic, heterozygous gene-corrected control cells were then engineered from the patient iPSCs with a strategy adapted from Yusa and colleagues (32) through zinc finger nuclease (ZFN)-stimulated homologous recombination (see Experimental Procedures). Genotypes of both the patient (343delT/343delT) and heterozygous wildtype knock-in control (WT

KI/343delT) iPSCs are outlined in Fig. 1B, and were confirmed through direct Sanger sequencing (Fig. 1C). Both iPSC lines expressed relevant pluripotency markers including NANOG, stage-specific embryonic antigen 4 (SSEA-4), octamer-binding protein 4 (OCT-4), and TRA-1-81 at the protein level (Fig. 1D-E) and *NANOG*, *OCT-4* (*POU5F1*), *SOX2*, and *TRA-1-60* at the RNA level (Fig. 1F). *In vitro* EZ sphere differentiations of both cell lines resulted in upregulation of markers from all three germ layers (Fig. 1G). Karyotypes were normal (Fig. 1H). These data validate the use of generated iPSC lines for further investigations.

343delT Protein is not Detectable in iSKMs or iCMs though RNA is Present— Validated iPSC lines were differentiated into skeletal myotubes (iSKMs) and cardiomyocytes (iCMs) using established protocols (see Experimental Procedures). iCMs contracted rhythmically in the dish, stained positive for cardiomyocyte markers including Troponin T (TnT) (Fig. 2A) and exhibited cardiomyocyte-like action potential profiles (Fig. 2C). iSKMs elongate as they mature in culture, many appear multi-nucleated, some cells can be observed to twitch spontaneously, and they stain positive for muscle markers including TnT (Fig. 2B and 4A) and desmin (Fig. 4B). No obvious phenotypic differences were observed between WT KI/343delT and 343delT/343delT iCMs or iSKMs when characterizing cell differentiation in this way.

The major difference observed between the muscle differentiated cell lines was a complete lack of detectable 343delT protein both through immunocytochemistry (Fig. 2A-B) and western blot (Fig. 2D-E) in the 343delT/343delT line when probed with and NT HSPB5 antibody. In the WT KI/343delT control, predicted to express both a 22 kDa-sized WT protein and a 15 kDa-sized 343delT protein, only the WT form of the protein is detectable (Fig. 2D-E), indicating lack of detectable 343delT is not due to immaturity of the cells. This result was surprising to us as the muscle biopsy from the patient showed dense, irregular staining of HSPB5 through immunohistochemistry and a 15 kDa-sized protein detectable by western blot with the NT HSPB5 antibody (29). Lack of 343delT protein was confirmed in a second iPSC line derived from the patient as well as the

isogenic, heterozygous gene-corrected control line derived from that iPSC line (Supplementary Figure S1). Additionally, homozygous knockin of the 343delT mutation into the endogenous *HSPB5* locus of an iPSC line derived from an unrelated, healthy individual also exhibited a complete lack of detectable 343delT protein (manuscript in preparation).

As 343delT protein was not detectable, we next investigated whether this was due to defects in RNA levels. The 343delT transcript is not predicted to be a target for nonsense-mediate mRNA decay (NMD) as the premature stop codon is downstream of the final exon-exon junction complex (33). Therefore we hypothesized 343delT transcript levels would be comparable to WT. Quantitative real-time PCR (qRT-PCR) of iCMs and iSKMs revealed expression of *HSPB5* mRNA in both WT KI/343delT and 343delT/343delT (Fig. 2F-G). *HSPB5* mRNA levels may differ depending on the efficiency of differentiation, which varies between iPSC lines and differentiation attempts, as noted by differences in expression of the muscle-specific gene *Troponin T* (*TNNT2*) (Fig. 2F-G). Therefore, though the level of *HSPB5* mRNA cannot be directly compared between samples, we confirm that 343delT mRNA is present. Additionally, in contrast to an unstable mRNA control, *MYC*, levels of *HSPB5* mRNA did not decline in WT KI/343delT or 343delT/343delT iCMs with treatment of actinomycin D to inhibit transcription over 24 hours (Supplementary Figure S2), indicating similar transcript stability between WT and 343delT. These results show the defect in 343delT protein expression is not due to deficient transcript levels.

Lack of 343delT Protein is not Due to Degradation, microRNA Targeting, or Defective Translation— To further investigate the reason for lack of 343delT protein detection, we next examined protein degradation as a possible mechanism. iCMs were treated with the proteasomal inhibitor MG132 (34), (Fig. 3A). In contrast to the increase in the short-lived cell cycle inhibitor p21 with MG132 treatment (35), 343delT protein (15 kDa) remained undetectable in both WT KI/343delT and 343delT/343delT with inhibition of proteasomal degradation. Inhibition of autophagosome maturation with bafilomycin A1 for 12 hours (36) was also insufficient to evoke

343delT protein detection in iCMs, though LC3-II (lower band) increased as expected with treatment (Supplementary Figure S3A). Additionally, treatment of 343delT/343delT iSKMs with the proteasomal inhibitor bortezomib for up to 48 hours (37) (Supplementary Figure S3B) or MG132 for 12 hours (Supplementary Figure S3C) and inhibition of autophagosome maturation with bafilomycin A1 for 12 hours (Supplementary Figure S3C) were also insufficient to evoke 343delT detection. These data suggest that the lack of detectable 343delT protein is not due to degradation by the proteasome or autophagy. Complimentary experiments of overexpression of 343delT in a human breast cancer cell line (MCF7 cells), showed that both inhibition of the proteasome (MG132) and autophagy (bafilomycin A1) resulted in slight increases of 343delT protein (Supplementary Figure S3D-E). This result suggests that 343delT protein is likely degraded to some extent by the proteasome and autophagy, but this is not the major cause for our inability to detect 343delT protein in our iPSC model.

Another possibility we considered is that 343delT mRNA is differentially targeted compared with WT by a microRNA that inhibits translation. To examine this possibility, we transfected iCMs with siRNA to knockdown dicer, the protein responsible for processing pre-microRNAs into mature microRNAs (38). Though knockdown of dicer was confirmed through decreased levels of dicer protein and elevated levels of c-MYC, a known target of dicer-dependent microRNAs (39), we were unable to detect 343delT protein in either WT KI/343delT or 343delT/343delT (Fig. 3B). This result suggests that 343delT is not differentially targeted by a dicer-dependent microRNA.

To confirm there is no inherent defect in the translation efficiency of 343delT compared with WT, we performed an *in vitro* transcription/translation assay using rabbit reticulocyte lysate labeling translated proteins with ^{35}S-L-methionine and ^{35}S-L-cysteine. We utilized a plasmid containing N-terminally MYC-tagged versions of WT (pCS2-MYC-WT) and 343delT (pCS2-MYC-343delT) and an SP6 promoter as the template for this reaction. Both WT and 343delT are visible after 30 minutes of incubation and increase after 90 minutes (Fig. 3C). No significant

difference is observed between WT and 343delT in the rate of synthesis over time (21.8 ± 3.4 and 19.1 ± 6.9, respectively) of the recombinant protein. This result shows 343delT is translated efficiently, at least in this reticulocyte lysate.

In toto, these results demonstrate that lack of detectable 343delT protein in iCMs and iSKMs generated from 343delT/343delT and WT KI/343delT is not attributable to proteasomal degradation, autophagic degradation, microRNA targeting, or defective translation.

343delT Forms Insoluble Protein Aggregates and Induces a Cellular Stress Response when Overexpressed— The results presented above utilizing iCMs and iSKMs show an absence of detectable 343delT protein. The presence of mutant protein in the patient's biopsy specimen suggests that accumulation of 343delT in the affected tissue may contribute to disease. For this reason, we attempted to simulate these conditions with our model to determine if high levels of 343delT expression would result in aggregation in muscle cells.

We transiently transfected N-terminally MYC-tagged WT or 343delT constructs (pCMV-MYC-WT and pCMV-MYC-343delT) into 343delT/343delT iSKMs. Overexpression of 343delT resulted in aggregation in iSKMs marked by TnT (Fig. 4A) or desmin (Fig. 4B), whereas overexpression of WT resulted in diffuse, cytoplasmic staining (Fig. 4A-B). 343delT aggregates exclude TnT and desmin. Similar aggregates of 343delT were observed with overexpression in 343delT/343delT iCMs (data not shown). These results indicate that at high levels, 343delT forms aggregates in muscle cells.

Since overexpression of 343delT in iSKMs recapitulates aggregation observed in the patient's biopsy, we examined if overexpression in non-muscle cell lines also results in 343delT aggregation. Transfection is difficult in iCMs and iSKMs and variances in differentiation efficiency may impact results, making overexpression studies in commercially available cells lines that lack endogenous HSPB5 expression, such as BHK21 cells (baby hamster kidney fibroblasts), more appealing. Overexpression of pCMV-MYC-343delT forms cytoplasmic aggregates in BHK21 cells (Fig. 4C), which are detectable with both NT HSPB5 and MYC-tag antibodies. Absence of

additional cells staining with NT HSPB5 relative to MYC-tag exemplifies the lack of endogenous HSPB5 expression. Aggregates in BHK21 cells typically appear in the perinuclear region and look similar to aggregates observed with overexpression in iSKMs (Fig. 4A-B). Overexpression of pCMV-MYC-WT in BHK21 cells results in diffuse, cytoplasmic staining (Fig. 4C). These experiments provide proof-of-concept for the use of overexpression of 343delT in BHK21 cells as a platform to investigate 343delT aggregation and protein dynamics.

We noted that levels of 343delT protein expression were consistently lower than WT by immunocytochemistry and western blot when overexpressed in all cell lines tested. We confirmed equal transfection efficiency through co-transfection with a pCMV-dsRed plasmid (data not shown). Additionally, levels of WT and 343delT mRNA were assessed between 2-24 hours after transfection and determined to be similar (Supplementary Figure S4A). RNA levels correlated with transfection efficiency for the WT construct (Supplementary Figure S4B). Transfection with either WT or 343delT neither impacted cell proliferation nor viability (Supplementary Figure S5A-B) when compared with empty vector (EV) transfection over a similar period. These results indicate transfection efficiencies and RNA levels were equal and cell proliferation and viability were unaffected by transfection.

The metastable desmin protein is a known client for HSPB5 (12-14) and is present in aggregates in patients with desmin-related (cardio-) myopathy (25,26,40). Though 343delT aggregates did not colocalize with desmin in iSKMs, we wanted to examine this in BHK21 cells, which express endogenous desmin as well (26,31). 343delT aggregates in BHK21 cells colocalize with desmin in some (Fig. 4D, middle panel), but not all cells (Fig. 4D, bottom panel), potentially indicating stochastic incorporation of desmin into aggregates.

Misfolded proteins and protein aggregates are triggers for the induction of a cellular stress response driven by the master regulatory transcription factor HSF1(41). This response results in the upregulation of genes whose promoters contain heat shock response elements

including HSP70 (as reviewed in (2)). Indeed, overexpression of 343delT in BHK21 cells resulted in induction of HSP70 in some, but not all, transfected cells (Fig. 4E), while WT does not result in HSP70 induction (Fig. 4E). We further confirmed this induction by western blot (Fig. 4F). These results indicate that 343delT can induce a cellular stress response when overexpressed. Consistent upregulation of HSP70 in 343delT/343delT iCMs under basal conditions was not observed (data not shown), indicating perhaps the detectable, aggregated form of 343delT and/or the presence of other proteins in the aggregates is required for upregulation of HSP70.

Altogether, these results show the ability of 343delT to form visible, cytoplasmic aggregates when overexpressed in muscle and non-muscle cells, with potentially stochastic incorporation of desmin into these aggregates, at least in non-muscle cells. Additionally, HSP70 induction demonstrates disruption in overall protein homeostasis with overexpression of 343delT.

Co-Expression with WT Solubilizes 343delT— As 343delT is a recessively inherited mutation, in order to mimic the unaffected heterozygous parents, we co-transfected HA-tagged WT and MYC-tagged 343delT constructs (pCMV-HA-WT HSPB5 and pCMV-MYC-343delT HSPB5) into cell lines in equimolar ratios. In the presence of WT, 343delT no longer forms aggregates in BHK21 cells (Fig. 5A, bottom panel). Additionally, when expressed alone, 343delT was present almost entirely in the insoluble fraction ($99 \pm 1\%$, mean $\pm$ s.d., n=3), while when co-expressed with WT, the percent insoluble 343delT was reduced 6.6 fold ($15 \pm 6\%$, mean $\pm$ s.d., n=3, p-value of <0.01 as calculated by student's t-test) (Fig. 5B-C). The percentage of insoluble 343delT was quantified using the 15 kDa-sized band ([insoluble] $_{density}$ *100 / ([insoluble] $_{density}$ + [soluble] $_{density}$)). Larger molecular weight bands may be post-translationally modified forms of the protein; inclusion of these bands in analysis does not impact relative percent insoluble 343delT. These results indicate that the presence of WT shifts 343delT from the insoluble to the soluble fraction.

To determine if 343delT and WT are interacting, we co-transfected HA-tagged WT and MYC-tagged 343delT and performed co-immunoprecipitation (Co-IP). IP of HA resulted in the pull down of MYC-tagged 343delT only in the co-transfected sample (Fig. 5D). Reciprocally, IP of MYC resulted in the pull down of HA-tagged WT only in the co-transfected sample (Fig. 5D). The insoluble pellet fraction demonstrated that much of the 343delT protein, when transfected alone, was insoluble (Fig. 5D), consistent with the idea that WT solubilizes 343delT. These results demonstrate an interaction between WT and 343delT proteins within the cell.

343delT Solubility: In vitro and In vivo— In line with overexpression in mammalian cell lines, the overexpression of recombinant 343delT in *E.coli* resulted in an insoluble product exclusively found in inclusion bodies (Fig. 6A). Refolding of 343delT in the absence of WT predominantly led to the formation of insoluble aggregates (Fig. 6B). Conversely, the presence of an excess of WT during the entire refolding process resulted in the formation of a soluble product (Fig. 6B). This mixture eluted from gel filtration in a single peak with a slight shoulder at an elution volume of approximately 10 mL, slightly earlier than refolded WT, which eluted at 10.5 mL (Fig. 6C). SDS-PAGE of the resulting fractions showed the co-elution of 343delT (14.7 kDa) with WT (20.2 kDa) across the entire peak, whilst only a single band at the WT mass was visible in the control (Fig. 6C, upper panel). To obtain a higher resolution view of the oligomers formed, we performed native mass spectrometry (42). A spectrum of WT reveals a broad region of signal centered around 10,000 *m/z*, resulting from the overlap of a large number of charge states (Fig. 6D), and consistent with a polydisperse ensemble of oligomers (43). A spectrum obtained for the 343delT:WT mixture at identical mass spectrometry conditions reveals an additional charge series at approximately 2,000 *m/z*, corresponding to a mass of 14,695 Da, which can be assigned to the monomeric form of 343delT (Fig. 6D). Interestingly, the charge states populated are relatively low, indicative of a largely folded conformation of the 343delT monomers free in solution. Examination of the high *m/z* region of the spectrum for WT allows the assignment of overlapping charge-state envelopes to the oligomers comprising the ensemble.

6

Strikingly, many additional features are observed in the spectra for the 343delT:WT mixture (Fig. 6D, insert). The complexity of the spectrum is such that individual oligomers cannot be directly identified, but by comparison to the WT data it is clear that they cannot be explained by integer stochiometries of WT HSPB5, but rather that an ensemble of heteroligomers is present, resulting from a direct interaction between the two proteins. These *in vitro* data further support the notion that WT solubilizes 343delT through a direct interaction.

We hypothesized that extreme insolubility of 343delT was responsible for our inability to detect the mutant protein in iSKMs and iCMs, and for lower levels of 343delT compared with WT upon overexpression. We have excluded many reasons for the absence of detectable 343delT protein noted above, including mRNA instability, degradation by the proteasome or autophagy, targeting by a dicer-dependent microRNA, and defective translation. Decreased detectable 343delT protein compared with WT was consistently observed both through analyses by western blot and immunocytochemistry. We tested additional lysis buffers to determine if we could detect 343delT by western blot including RIPA buffer, 100% formic acid, and 8 M urea plus 2% SDS. We observed a consistent lack of 343delT protein in iCMs with all tested buffers (data not shown).

Addition of a small ubiquitin-related modifier (SUMO) to proteins has been shown to enhance their solubility (44,45). To directly test our hypothesis that insolubility of 343delT is the reason for low levels of detection with overexpression, we generated SUMO-HSPB5 fusion constructs. These plasmids contain a version of WT and 343delT HSPB5 that are N-terminally MYC-tagged followed by SUMO, preceding the HSPB5 variant. We used a non-cleavable version of SUMO3 Q89P (46) in this construct to prevent removal of SUMO by endogenous deSUMOylases. MYC-tag only versions of the constructs were used as controls. Expression of SUMOylated constructs in BHK21 cells results in a 130 ± 60 and 5 ± 1 (mean $\pm$ s.d.) fold increase in 343delT and WT, respectively (Fig. 6E). The larger increase of 343delT compared with WT through the addition of SUMO

($p<0.05$, calculated by student's t-test) suggests that the increase in mutant protein is likely not due to inherent stabilization and/or enhanced transcription/translation of proteins by SUMO addition; if this were the case, similar increases in WT and 343delT would be expected. Elevated detection of 343delT was also observed with overexpression of 343delT and SUMOylated 343delT in 343delT/343delT iCMs resulting in 811 ± 218 fold (mean $\pm$ s.d.) enhanced detection of the SUMOylated protein by western blot (Fig. 6F). These results suggest that our suboptimal ability to detect 343delT is due to extreme insolubility of the mutant protein in both non-muscle and muscle cells.

DISCUSSION

Altogether, the data presented here describe molecular defects observed with disease-causing 343delT. Although mRNA is unaffected, basal levels of 343delT protein in iCMs or iSKMs were undetectable in both WT KI/343delT and 343delT/343delT cell lines. Detection of the WT-sized protein, but not the truncated 343delT-sized protein in the heterozygous WT KI/343delT iPSC-derived cells indicates that absence of 343delT is not due to lack of maturation. Several possibilities such as, proteasomal degradation, autophagic degradation, Dicer-dependent microRNA targeting, and inherent translational defects were examined and proved unlikely mechanisms responsible for lack of detectable 343delT protein. Overexpression of 343delT consistently resulted in much lower levels of protein compared with WT as well. Greatly enhanced detection of 343delT when fused to SUMO3 Q89P, a non-cleavable form of SUMO known to enhance protein solubility, is consistent with extreme insolubility of 343delT as the reason for lack of protein detection.

It is conceivable that insoluble 343delT would be unavailable to perform essential, normal functions of HSPB5 in the muscle cells, suggestive that loss of HSPB5 function contributes to myopathy in the patient harboring homozygous 343delT. HSPB5 specifically plays key chaperone roles for proteostasis and protein quality control, differentiation, and maintenance in muscle cells (12-23). Loss of these or other functions of HSPB5 may leave myotubes vulnerable to stress,

7

prone to muscle breakdown with increased usage, and/or have an impact on regeneration of skeletal muscle from satellite cells. Although absent at presentation, the early onset of the skeletal myopathy in the patient does not preclude later development of cardiac manifestations.

Though 343delT protein is observed in the patient skeletal muscle biopsy, it does appear at lower levels when compared with a control individual (29). Nonetheless, endogenous detection of the mutant protein was not observed in our iPSC-derived cells. Potentially our model does not recapitulate 343delT expression observed in the patient for reasons related to the culture environment (pH differences, 2D cell culture vs. 3D tissue structure, oxygen levels, etc.), stress (contraction, muscle turnover), variability in experimental techniques, age- and tissue-dependent, and other factors. This may illustrate inherent limitations of iPSCs in modeling diseases due to an accumulation of stressors over time, also corresponding to the observation that the patient was entirely normal until disease onset at 4 months of age. Therefore, we hypothesize that the iPSCs recapitulates what may have occurred early in the patient, i.e. prior to disease manifestation. 343delT may be packaged into a completely insoluble state when expressed at basal levels, and its accumulation over time could result in 343delT surpassing a threshold thereby allowing detection. The potential change in protein status may or may not contribute to disease. It is of interest that the severity and early onset nature of the autosomal recessive disease in the 343delT patient is not consistent with the DKO mouse (20), which develops progressive myopathy into adulthood. We recognize these differences could be due to species variation and/or the DKO mouse also lacking HSPB2. Alternatively, the presence of 343delT protein could exacerbate the phenotypes observed in the complete loss of function scenario (DKO mouse).

Co-aggregation of 343delT with desmin was observed upon overexpression of 343delT in some but not all BHK21 cells, but was not observed with overexpression in iSKMs. Other mutations in *HSPB5* such as R120G (26,40) result in co-aggregation of the mutant protein with desmin and patients are termed to have desmin-related (cardio-) myopathy. The stochastic

accumulation of desmin in 343delT aggregates is likely due to loss of 343delT chaperone function towards aggregation-prone desmin resulting in the two proteins clustered together, amongst other proteins, in aggregates. The extent of desmin accumulation in aggregates likely depends on overall protein homeostasis within the cell. The finding that overexpression of 343delT induced elevated levels of HSP70 in BHK21 cells is consistent with cells suffering from an imbalance in protein homeostasis. We did not observe consistently elevated HSP70 levels in 343delT/343delT iCMs under basal conditions, which indicates that the presence of detectable 343delT (i.e. the visible aggregated form) and potentially other proteins present in the aggregates are required for disruption of protein homeostasis.

The recessive nature of 343delT led us to investigate the interaction between 343delT and WT HSPB5. It is unknown if the heterozygous parents, who are non-consanguineous and healthy, express detectable levels of the 343delT protein. Potentially, expression of 343delT in the heterozygous state may not be detrimental as we have shown increased solubility of 343delT and loss of aggregate formation upon co-expression with equimolar WT. Our Co-IP experiments demonstrate an interaction between 343delT and WT within the cell. Together these data suggest that WT solubilizes 343delT. Additionally, the presence of WT during refolding of 343delT rescues the protein from forming insoluble aggregates *in vitro*. The shift in elution volume during size exclusion and co-elution of the proteins as observed by SDS-PAGE suggest the formation of a complex between WT and 343delT, which is confirmed directly by native mass spectrometry experiments. The observation of a large proportion of what appears, from the absence of highly charged 343delT species, to be solution phase monomeric 343delT in the mass spectrum suggests a labile interaction, especially under the conditions used, consistent with a chaperone-like interaction. The ability of WT to solubilize 343delT and the presence of unaffected WT protein to perform normal cellular functions likely result in the parents being asymptomatic.

Overall our data support loss of HSPB5 function as a likely mechanism contributing to the myopathy. Given the substantial number of protein

8

aggregation diseases, the findings reported here have direct implications for understanding the mechanisms of variable expressivity of both disease susceptibility and resistance. Though we cannot exclude the presence of the mutant protein directly contributing to disease, any detrimental effects of the 343delT protein would likely be ameliorated by the presence of WT through solubilization. Exogenous expression of WT HSPB5 by a gene therapy approach may therefore improve symptoms in mutant HSPB5-induced myopathy. Design of effective delivery methods for exogenous chaperones to the tissue or gene/cell therapy would be necessary for this treatment.

EXPERIMENTAL PROCEDURES

Reprogramming Patient Dermal Fibroblasts to iPSCs— Dermal fibroblasts were isolated from the patient containing the 343delT mutation (29) with written consent of the patient's mother and with research ethics committee approval at Guy's & St Thomas' NHS Foundation Trust (London, UK) for biobank storage and transfer of samples for use in an ethically approved research project. Fibroblast culture and further research in the laboratory was performed with appropriate IRB approval at the University of Utah (Salt Lake City, UT) and the Medical College of Wisconsin (Milwaukee, WI) for use of human cells. Dermal fibroblasts expanded in DMEM supplemented with 10% FBS and 100 u penicillin/100ug streptomycin/ml media (P/S) (all from Life Technologies) were reprogrammed into induced pluripotent stem cells (iPSCs) through transduction with 4 retroviruses carrying the genes *OCT-4*, *SOX2*, *c-MYC*, and *KLF4* as previously described (30). Following transduction, transduced fibroblasts were seeded onto SNL feeder cells (Cell Biolabs) that were mitotically inactivated through treatment with Mitomycin C (ATCC), in ESC medium composed of Knockout DMEM supplemented with 20% Knockout Serum Replacement, Minimum Essential Medium-Non-Essential Amino Acids (MEM-NEAA), 2 mM L-glutamine (all from Life Technologies), P/S, 0.1 mM β-mercaptoethanol (Sigma), 10 ng/ml human bFGF (Cell Signaling), and 50 ng/ml L-ascorbic acid (Sigma). Resulting iPSC clones were manually picked and maintained on feeder cells in ESC medium for four passages before

transitioning to feeder-free culture as described below.

iPSC Culture— iPSCs were routinely cultured in feeder-free conditions on matrigel (Corning)-coated dishes with mTeSR1 (Stem Cell Technologies) or StemMACS iPS-Brew XF (Miltenyi Biotec). Cells were passaged every 3-4 days using Accutase (Life Technologies) and seeded in media containing 10 μM ROCK inhibitor (Y-27632, Selleck) for 24 hours following passaging.

Gene-Editing in iPSCs, Genotyping, and Sequencing— iPSCs derived from the homozygous recessive 343delT patient (343delT/343delT) were gene-corrected to generate heterozygous 343delT iPSCs (WT KI/343delT) using a protocol modified from a previously defined strategy that involves knockin/excision of a selection cassette (32). Briefly, zinc finger nucleases (ZFNs) were designed and generated by Sigma (CompoZr Custom Zinc Finger Nucleases). The targeting vector was designed and synthesized using Gene Art (Life Technologies) containing a portion of the WT *HSPB5* sequence with a silent mutation (435 G>T) to generate a TTAA site for *piggyBac* excision. The puromycin/thymidine kinase selection cassette driven by the PGK promoter (PGK-*puroΔtk*) and flanked by *piggyBac* repeats was cloned from the pPB-CAG-OSKM-puDtk vector (Sanger Institute, UK) into the targeting vector through In-Fusion Cloning (CloneTech). Components were transfected into iPSCs using a 4D-Nucleofector and P4 Nucleofector Solution with program CB-150 (Lonza) followed by seeding onto SNL feeder cells and selection with 0.5-1 μg/ml puromycin (InvivoGen) from days 5-12 post-transfection. Resulting puromycin resistant clones were manually picked and genotyped. Heterozygous knockin clones were selected for excision of the selection cassette and transfected with an excision only *piggyBac* transposase (PBx, Transposagen) followed by negative selection with 0.5 μM Ganciclovir (Cayman Chemicals). Resulting colonies were picked and genotyped. PCR products from WT KI/343delT iPSCs were cloned into a TOPO vector (Life Technologies) and plasmids were isolated from bacterial colonies and Sanger sequenced by Retrogen (San Diego, CA) to

9

confirm heterozygosity for the 343delT mutation and incorporation of the engineered silent mutation. WT KI/343delT iPSCs were expanded and transitioned to feeder-free culture as described above.

Immunocytochemistry— Cells on 4% paraformaldehyde (Sigma) fixed glass coverslips were permeabolized with 0.1% triton-X 100 (Sigma), blocked with 3% bovine serum albumin (Ultrapure BSA- Cell Signaling), and stained appropriately before finally mounting with Ultracruz Hard Set Mounting Media plus DAPI (Santa Cruz). Primary antibodies: NANOG (Cell Signaling 4903p, 1:200), SSEA-4 (Stem Cell Technologies 60062AD, 1:40), OCT-4 (Cell Signaling 2840, 1:400), TRA-1-81 (Abcam ab16289, 1:100), N-terminal (NT) HSPB5 (NovaCastra ABCrys513, Leica, 1:100), troponin T (TnT, Abcam 45932, 1:500), MYC-tag (Cell Signaling 2278, 1:100), desmin (Dako M0760, 1:100), HSP70 (Stress Marq SMC-100A/B, 1:100), and HA-tag (Invivogen ab-hatag, 1:500). Secondary antibodies: AlexaFluor 488 donkey anti-rabbit IgG and AlexaFluor 555 donkey anti-mouse IgG (Life Technologies, 1:500). Images were taken on a Nikon A1 confocal microscope.

Quantitative Real-Time PCR (qRT-PCR)— RNA was isolated using PureLink RNA MiniPrep Kit (Life Technologies) followed by treatment with DNA-free DNA Removal Kit (Life Technologies). cDNA was generated using High-Capacity cDNA Reverse Transcription Kit (Life Technologies). qRT-PCR was performed using BioRad CFX 96 Thermocycler (BioRad) with Qiagen QuaniTect SYBR Green PCR Mix and QuantiTect Primer Assays (Qiagen). BioRad CFX Manager Software (BioRad) was used for data analysis.

Karyotyping—Performed by Wisconsin Diagnostic Laboratories (formerly Dynacare Laboratories) (Milwaukee, WI).

iCM and iSKM Differentiation— iCM differentiation was performed using chemical modulation of the Wnt pathway modified from a previously described protocol (47). Briefly, iPSCs at 100% confluency were overlayed with matrigel in mTeSR1 or StemMACS iPS-Brew XF media on Day-1. D0, cells were treated with 12 μmol/L Chir-99021 (Selleck) and 10 ng/ml human Activin-A (R & D Systems) in RPMI minus insulin medium (RPMI supplemented with 1X B27 supplement minus insulin- both from Life Technologies). Day 2, media was changed to RPMI minus insulin. Day 3, cells were treated with 5 μmol/L IWP-2 (Stem Cell Technologies) in RPMI minus insulin, with media subsequently changed on Day 5 to RPMI minus insulin. Media was changed to Complete medium, RPMI supplemented with 1X B27 supplement (Life Technologies) and P/S on Day 7 and changed every 2-3 days following until cells were utilized for experiments around Day 30 of differentiation. iCMs were passaged prior to experiments using TrypLE Express (Life Technologies) and seeded in Complete medium containing 10% FBS and 10 μM ROCK inhibitor on 0.1% gelatin-coated surfaces.

iSKMs were differentiated using the EZ sphere protocol as previously described (48). Week 5 EZ spheres where treated with Accutase and pelleted for qRT-PCR of markers for all three germ layers. Week 6 EZ spheres were terminally differentiated as previously described (48) for 3 weeks prior to experiments. Immunocytochemistry was performed directly on cells differentiated on coverslips.

Electrophysiology of iCMs—Action potentials were recorded using intracellular sharp electrodes. Coverslips containing beating clusters of iCMs were placed in Tyrodes solution and held at physiological temperature with a heated recording chamber (TC-344B; Warner Instruments). Sharp electrodes were pulled from borosilicate glass (FHC, Inc.) using a Sutter Model P-97 to resistances of 50-70 MΩ when backfilled with 3M KCl. Recordings were acquired using a Multiclamp 700B amplifier (Molecular Devices) interfaced with a Digidata 1449A (Molecular Devices). The pClamp software suite (version 10; Molecular Devices) was used for data acquisition and analysis. Graphing of representative action potentials was performed using Origin software (OriginLab).

Cell Fractionation Assay and Western Blot—Detergent soluble, detergent insoluble, and whole cell lysate (WCL) fractions were isolated and western blots performed as described previously (49), except equal amounts of protein were separated on Mini-Protean TGX Gels 4-20% (BioRad). Primary antibodies: NT HSPB5

10

(NovaCastra ABCrys513, Leica, 1:100), GAPDH (Cell Signaling 2118, 1:10,000), p21 (Santa Cruz sc-sc397, 1:250), LC3 (Novus NB100-2220, 1:10,000), dicer (SantaCruz sc-393328, 1:100), c-MYC N-262 (Santa Cruz sc-764, 1:500), MYC 9E10 (Santa Cruz sc-40, 1:200), HSP70 (Stress Marq SMC-100A/B, 1:1,000), α-tubulin (Santa Cruz sc-5546, 1:500), β-actin (Abcam ab6276, 1:5,000), and HA-tag (Invivogen ab-hatag, 1:1,000). Quantification of band intensity was performed using Image J or Image Lab 5.2.1 (BioRad) software.

Inhibition of the Proteasome and Autophagosome Maturation— iCMs and iSKMs were treated with DMSO, 10 μM MG132 or 10 or 100 nM bortezomib to inhibit the proteasome, or 80nM bafilomycin A1 to inhibit autophagosome maturation for 12 hours.

Dicer Knockdown— iCMs were transfected with scrambled siRNA control (-), or either 40 pmols (+) or 80 pmols (++) siRNA targeting dicer (SantaCruz) using Lipofectamine RNAi Max (Life Technologies). Samples were harvested 72 hours post-transfection.

HSPB5 Vector Constructs— pCMV N-terminal MYC-tagged WT and HA-tagged WT (pCMV-MYC-WT and pCMV-HA-WT, respectively) were generated previously (49). The pCMV-MYC-343delT construct was produced by *in vitro* site-directed mutagenesis as described previously (49). MYC-WT and MYC-343delT were PCR-amplified from pCMV-MYC vectors and cloned into a pCS2 vector, which contains an SP6 promoter required for TNT assay (see below). For SUMOylated constructs, a gBlock Gene Fragment (Integrated DNA Technologies) was purchased containing the non-cleavable SUMO3 Q89P sequence obtained from the pcDNA3 MYC-SUMO3Q89P vector (Addgene Plasmid #48963) (46), and cloned into pCMV-MYC-WT and 343delT constructs. Resulting constructs, pCMV-MYC-SUMO3 Q89P-WT and pCMV-MYC-SUMO3 Q89P-343delT, are a fusion in the N to C terminal direction of MYC-SUMO3Q89P-WT and 343delT HSPB5, respectively.

In vitro Transcription/Translation Assay— TNT SP6 Quick Coupled Transcription/Translation Systems (Promega) was used with EXPRE^{35}S^{35}S Protein Labeling Mix (PerkinElmer) containing both ^{35}S-L-methionine

and ^{35}S-L-cysteine. pCS2-MYC-WT and 343delT plasmids were used as template DNA in the reaction according to the manufacturer's instructions. Samples were subsequently run on a 12% SDS-PAGE gel, transferred to nitrocellulose membranes, and exposed to film at -80ºC. Quantification of band intensity was performed using Image J software.

Transfection—iSKMs were transfected using Lipofectamine 3000 (Life Technologies) according to the manufacturer's instructions.

BHK21 cells (ATCC) were cultured in Glasgow media supplemented with 5% tryptose phosphate broth (both from Life Technologies), 15% FBS, and P/S. BHK21 cells were transfected with Lipofectamine 3000 according to the manufacturer's instructions. For co-transfection of two plasmids, equal amounts of each plasmid were used with empty vector (EV) plasmid added to single plasmid transfections to control for total DNA amount.

iCMs were passaged and resuspended in P3 nucleofection solution (Lonza) and transected using the CA-137 program on the 4D-Nucleofector System (Lonza). Following transfection, cells were seeded onto fibronectin-coated surfaces (Corning) in Complete media supplemented with 10% FBS and ROCK inhibitor.

Co-Immunoprecipitation—Cell pellets were resuspended in RIPA Buffer (Thermo Scientific) supplemented with Halt Protease and Phosphatase inhibitor (Thermo Scientific), sonicated on ice and centrifuged at 4ºC for 10 minutes at 12,000 x g. A portion was removed here for WCL, diluted with 4x XT Sample Buffer, and boiled 5 minutes. The remaining WCL was used for IP preformed with Protein G Sepharose 4 Fast Flow Beads (Genesee). Samples were pre-cleared through incubation with beads for 45 minutes on a rotisserie shaker at 4 ºC, followed by pre-incubation with 200 μg/ml antibody, either MYC 9E10 (Santa Cruz sc-40) or HA (Invivogen ab-hatag) for 30 minutes at 4ºC with intermittent vortexing. Beads were added to sample/antibody mixture and incubated on rotisserie shaker for 1 hour at 4ºC. Bead-bound samples were washed 6 times with RIPA buffer and finally resuspended in RIPA buffer with 4x XT Sample Buffer, boiled 5 minutes, and centrifuged 30 seconds at 12,000 x g. The insoluble pellet, prior to IP, was washed 2

11

times with RIPA buffer, resuspended in 4x XT Sample Buffer, boiled 5 minutes, and centrifuged 30 seconds at 12,000 x g. All fractions were loaded onto Mini-Protean TGX Gels 4-20% (BioRad). Western blots were performed as described above.

In vitro 343delT Protein Expression, Refolding and Purification— The 343delT plasmid, purchased from GenScript, was transformed into BL21 (DE3) Stratagene Gold Competent cells (Agilent Technologies) and plated on kanamycin selective plates. A single colony was picked and used to inoculate 5mL of LB (Fisher). This culture was incubated at 37ºC, 220 rpm, overnight until a high OD was achieved. 1 L LB were then inoculated with 10 mL of the overnight culture and grown at 37ºC, 200 rpm, until an OD of between 0.6-0.8 was obtained. To induce 343delT expression a final concentration of 0.5 mM IPTG (Merck) was added and cultures grown for a further 3 hours before harvesting by centrifugation. Cell pellets were then stored at -80ºC for future use. Cells were thawed, re-suspended and lysed in 50 mM Tris (Sigma), 0.1mM EDTA (Sigma), 0.1 mM DTT (Sigma), 0.1 M NaCl (Sigma), 5% glycerol (Fisher), pH 7.9 (lysis buffer) containing a cOmplete EDTA free protease inhibitor tablet (Roche). Post-clarification overexpressed 343delT was shown to reside within insoluble inclusion bodies (IB) and not within the soluble lysate. The insoluble pellet was re-suspended in lysis buffer and any remaining cells were lysed by an additional sonication step. Membrane elements were solubilized by the addition of a final concentration of 1% Triton X-100 (Promega). This preparation was left to incubate for 15 minutes on ice before centrifugal

clarification. Two further washes of the IB pellet were carried out in lysis buffer to remove the remaining Triton X-100. Clean IB pellets were then solubilized in 6 M GuHCl (Sigma), 50 mM Tris, 0.1 mM EDTA, 0.1 mM DTT, 5% glycerol, pH 7.9 and agitated at room temperature for 1 hour, with any remaining insoluble material being removed by centrifugation. The protein concentration of the sample was estimated from UV absorbance measurements and 2 molar equivalence of WT HSPB5 was added. Protein refolding was achieved by gradually reducing the concentration of GuHCl by stepwise dialysis, initially to 2 M, 1 M and then 0 M to ensure refolding was complete. Samples were passed through a 0.22 µM Spin X Centrifuge tube (Fisher Scientific) and loaded onto a Superdex 200 10/300 column (GE Healthcare) to further purify and buffer exchange into 200 mM ammonium acetate (Sigma) pH 6.9. Fractions could then be analyzed by SDS-PAGE before being selected for mass spectrometry analysis.

Mass Spectrometry— Complex-containing samples were analyzed by nanoelectrospray mass spectrometry without the need for further sample preparation or concentration. Transmission pressures and energies on a Synapt G1 HDMS (Waters Corp) were optimized to preserve non-covalent interactions but to maintain the transmission of large assemblies. Spectra were obtained using a previously defined protocol (42) under the following conditions: capillary 1.5 kV, cone 50 V, extractor 3.0 V, trap 8.0 V, transfer 8.0 V, analyzer pressure 1.58 e^{-3} mBar, backing pressure 5.8 e^{0} mBar. All spectra were processed and analyzed in MassLynx V4.1.

Conflict of interest: The authors declare that they have no conflicts of interest with the contents of this article.

13

REFERENCES

1.	Morimoto, R. I. (1998) Regulation of the heat shock transcriptional response: cross talk between a family of heat shock factors, molecular chaperones, and negative regulators. *Genes & development* **12**, 3788-3796

2.	Christians, E. S., Yan, L. J., and Benjamin, I. J. (2002) Heat shock factor 1 and heat shock proteins: Critical partners in protection against acute cell injury. *Crit Care Med* **30**, S43-S50

3.	Gopal-Srivastava, R., and Piatigorsky, J. (1993) The murine alpha B-crystallin/small heat shock protein enhancer: identification of alpha BE-1, alpha BE-2, alpha BE-3 and MRF control elements. *Molecular and cellular biology* **13**, 7144-7152

4.	Gopal-Srivastava, R., Haynes II, J. I., and Piatigorsky, J. (1995) Regulation of the Murine aB-Crystallin/Small Heath Shock protein Gene in Cardiac Muscle. *Molecular and cellular biology* **15**, 7081-7090

5.	Poulain, P., Gelly, J. C., and Flatters, D. (2010) Detection and architecture of small heat shock protein monomers. *PloS one* **5**, e9990

6.	Hochberg, G. K., and Benesch, J. L. (2014) Dynamical structure of alphaB-crystallin. *Progress in biophysics and molecular biology* **115**, 11-20

7.	Hochberg, G. K., Ecroyd, H., Liu, C., Cox, D., Cascio, D., Sawaya, M. R., Collier, M. P., Stroud, J., Carver, J. A., Baldwin, A. J., Robinson, C. V., Eisenberg, D. S., Benesch, J. L., and Laganowsky, A. (2014) The structured core domain of alphaB-crystallin can prevent amyloid fibrillation and associated toxicity. *Proc Natl Acad Sci U S A* **111**, E1562-1570

8.	Peschek, J., Braun, N., Rohrberg, J., Back, K., Kriehuber, T., Kastenmüller, A., Weinkauf, S., and Buchner, J. (2013) Regulated structural transitions unleash the chaperone activity of αB-crystallin. *Proceedings of the National Academy of Sciences*, 201308898

9.	Rajagopal, P., Tse, E., Borst, A. J., Delbecq, S. P., Shi, L., Southworth, D. R., and Klevit, R. E. (2015) A conserved histidine modulates HSPB5 structure to trigger chaperone activity in response to stress-related acidosis. *eLife* **4**

10.	Clark, A. R., Naylor, C. E., Bagneris, C., Keep, N. H., and Slingsby, C. (2011) Crystal structure of R120G disease mutant of human alphaB-crystallin domain dimer shows closure of a groove. *Journal of molecular biology* **408**, 118-134

11.	Mainz, A., Peschek, J., Stavropoulou, M., Back, K. C., Bardiaux, B., Asami, S., Prade, E., Peters, C., Weinkauf, S., Buchner, J., and Reif, B. (2015) The chaperone alphaB-crystallin uses different interfaces to capture an amorphous and an amyloid client. *Nature structural & molecular biology*

12.	Houck, S. A., Landsbury, A., Clark, J. I., and Quinlan, R. A. (2011) Multiple Sites in alphaB-Crystallin Modulate its Interaction with Desmin Filaments Assembled *In Vitro*. *PloS one* **6**, e25859

13.	Perng, M. D., Cairns, L., Vandenijssel, P., Prescott, A., Hutcheson, A. M., and Quinlan, R. A. (1999) Intermediate filament interactions can be altered by HSP27 and alphaB-crystallin. *Journl of Cell Science* **112**, 2099-2112

14.	Bennardini, F., Wrzosek, A., and Chiesi, M. (1992) Alpha B-crystallin in cardiac tissue. Association with actin and desmin filaments. *Circulation Research* **71**, 288-294

15.	Bullard, B., Ferguson, C., Minajeva, A., Leake, M. C., Gautel, M., Labeit, D., Ding, L., Labeit, S., Horwitz, J., Leonard, K. R., and Linke, W. A. (2004) Association of the chaperone alphaB-crystallin with titin in heart muscle. *The Journal of biological chemistry* **279**, 7917-7924

16.	Golenhofen, N., Arbeiter, A., Koob, R., and Drenckhahn, D. (2002) Ischemia-induced association of the stress protein alpha B-crystallin with I-band portion of cardiac titin. *Journal of molecular and cellular cardiology* **34**, 309-319

17. Golenhofen, N., Perng, M. D., Quinlan, R. A., and Drenckhahn, D. (2004) Comparison of the small heat shock proteins alphaB-crystallin, MKBP, HSP25, HSP20, and cvHSP in heart and skeletal muscle. *Histochemistry and cell biology* **122**, 415-425

18. Kotter, S., Unger, A., Hamdani, N., Lang, P., Vorgerd, M., Nagel-Steger, L., and Linke, W. A. (2014) Human myocytes are protected from titin aggregation-induced stiffening by small heat shock proteins. *The Journal of cell biology* **204**, 187-202

19. Singh, B. N., Rao, K. S., Ramakrishna, T., Rangaraj, N., and Rao Ch, M. (2007) Association of alphaB-crystallin, a small heat shock protein, with actin: role in modulating actin filament dynamics in vivo. *Journal of molecular biology* **366**, 756-767

20. Brady, J. P., Garland, D. L., Green, D. E., Tamm, E. T., Giblin, F. J., and Wawrousek, E. F. (2001) aB-Crystallin in Lens Development and Muscle Integrity: A Gene Knockout Approach. *IOVS* **42**, 2924-2934

21. Morrison, L. E., Whittaker, R. J., Klepper, R. E., Wawrousek, E. F., and Glembotski, C. C. (2004) Roles for αB-crystallin and HSPB2 in protecting the myocardium from ischemia-reperfusion-induced damage in a KO mouse model. *American journal of physiology. Heart and circulatory physiology* **286**, H847-H855

22. Kumarapeli, A. R., Su, H., Huang, W., Tang, M., Zheng, H., Horak, K. M., Li, M., and Wang, X. (2008) Alpha B-crystallin suppresses pressure overload cardiac hypertrophy. *Circ Res* **103**, 1473-1482

23. Neppl, R. L., Kataoka, M., and Wang, D. Z. (2014) Crystallin-alphaB Regulates Skeletal Muscle Homeostasis via Modulation of Argonaute2 Activity. *The Journal of biological chemistry* **289**, 17240-17248

24. Christians, E. S., Ishiwata, T., and Benjamin, I. J. (2012) Small heat shock proteins in redox metabolism: implications for cardiovascular diseases. *The international journal of biochemistry & cell biology* **44**, 1632-1645

25. Mitzelfelt, K. A., and Benjamin, I. J. (2015) Multifunctional Roles of αB-Crystallin in Skeletal and Cardiac Muscle Homeostasis and Disease. in *The Big Book on Small Heat Shock Proteins* (Tanguay, R. M., and Hightower, L. E. eds.), 1 Ed., Springer International Publishing

26. Vicart, C. A., Guicheney, P., Li, Z., Prévost, M. C., Faure, A., Chateau, D., Chapon, F., Tomé, F., Dupret, J. M., Paulin, D., and Fardeau, M. (1998) A missense mutation in the alphaB-crystallin chaperone gene causes a desmin-related myopathy. *Nature genetics* **20**, 92-95

27. Elliott, J. L., Der Perng, M., Prescott, A. R., Jansen, K. A., Koenderink, G. H., and Quinlan, R. A. (2013) The specificity of the interaction between alphaB-crystallin and desmin filaments and its impact on filament aggregation and cell viability. *Philosophical transactions of the Royal Society of London. Series B, Biological sciences* **368**, 20120375

28. Wang, X., Osinska, H., Klevitsky, R., Gerdes, A. M., Nieman, M., Lorenz, J., Hewett, T., and Robbins, J. (2001) Expression of R120G- B-Crystallin Causes Aberrant Desmin and B-Crystallin Aggregation and Cardiomyopathy in Mice. *Circulation Research* **89**, 84-91

29. Forrest, K. M., Al-Sarraj, S., Sewry, C., Buk, S., Tan, S. V., Pitt, M., Durward, A., McDougall, M., Irving, M., Hanna, M. G., Matthews, E., Sarkozy, A., Hudson, J., Barresi, R., Bushby, K., Jungbluth, H., and Wraige, E. (2011) Infantile onset myofibrillar myopathy due to recessive CRYAB mutations. *Neuromuscular disorders : NMD* **21**, 37-40

30. Takahashi, K., Okita, K., Nakagawa, M., and Yamanaka, S. (2007) Induction of pluripotent stem cells from fibroblast cultures. *Nature protocols* **2**, 3081-3089

31. Christians, E. S., Banerjee Mustafi, S., and Benjamin, I. J. (2014) Chaperones and Cardiac Misfolding Protein Diseases. *Current Protein and Peptide Science* **15**

32. Yusa, K., Rashid, S. T., Strick-Marchand, H., Varela, I., Liu, P. Q., Paschon, D. E., Miranda, E., Ordonez, A., Hannan, N. R., Rouhani, F. J., Darche, S., Alexander, G., Marciniak, S. J., Fusaki, N.,

15

Hasegawa, M., Holmes, M. C., Di Santo, J. P., Lomas, D. A., Bradley, A., and Vallier, L. (2011) Targeted gene correction of alpha1-antitrypsin deficiency in induced pluripotent stem cells. *Nature* **478**, 391-394

33. Amrani, N., Sachs, M. S., and Jacobson, A. (2006) Early nonsense: mRNA decay solves a translational problem. *Nature reviews. Molecular cell biology* **7**, 415-425

34. Lee, D. H., and Goldberg, A. L. (1998) Proteasome inhibitors: valuable new tools for cell biologists. *Trends in Cell Biology* **8**, 397-403

35. Bloom, J., Amador, V., Bartolini, F., DeMartino, G., and Pagano, M. (2003) Proteasome-Mediated Degradation of p21 via N-Terminal Ubiquitinylation. *Cell* **115**, 71-82

36. Yamamoto, A., Tagawa, Y., Yoshimori, T., Moriyama, Y., Masaki, R., and Tashiro, Y. (1998) Bafilomycin A1 Prevents Maturation of Autophagic Vacuoles by Inhibiting Fusion between Autophagosomes and Lysosomes in Rat Hepatoma Cell Line, H-4-II-E Cells. *Cell Structure and Function* **23**, 33-42

37. Nawrocki, S. T., Carew, J. S., Dunner, K., Jr., Boise, L. H., Chiao, P. J., Huang, P., Abbruzzese, J. L., and McConkey, D. J. (2005) Bortezomib inhibits PKR-like endoplasmic reticulum (ER) kinase and induces apoptosis via ER stress in human pancreatic cancer cells. *Cancer research* **65**, 11510-11519

38. Flores-jasso, C. F., Arenas-huertero, C., Jose Luis, R., Contreras-cubas, C., Alejandra, C., and Vaca, L. (2009) First step in pre-miRNAs processing by human Dicer. *Acta Pharmacol Sin* **30**, 1177-1185

39. Jackstadt, R., and Hermeking, H. (2015) MicroRNAs as regulators and mediators of c-MYC function. *Biochimica et Biophysica Acta (BBA) - Gene Regulatory Mechanisms* **1849**, 544-553

40. Perng, M. D., Wen, S. F., van den, I. P., Prescott, A. R., and Quinlan, R. A. (2004) Desmin aggregate formation by R120G alphaB-crystallin is caused by altered filament interactions and is dependent upon network status in cells. *Mol Biol Cell* **15**, 2335-2346

41. Vabulas, R. M., Raychaudhuri, S., Hayer-Hartl, M., and Hartl, F. U. (2010) Protein folding in the cytoplasm and the heat shock response. *Cold Spring Harbor perspectives in biology* **2**

42. Kondrat, F. L., Struwe, W., and Benesch, J. P. (2015) Native Mass Spectrometry: Towards High-Throughput Structural Proteomics. in *Structural Proteomics* (Owens, R. J. ed.), Springer New York. pp 349-371

43. Aquilina, J. A., Benesch, J. L., Bateman, O. A., Slingsby, C., and Robinson, C. V. (2003) Polydispersity of a mammalian chaperone: mass spectrometry reveals the population of oligomers in alphaB-crystallin. *Proceedings of the National Academy of Sciences of the United States of America* **100**, 10611-10616

44. Peroutka, R. J., Elshourbagy, N., Piech, T., and Butt, T. R. (2008) Enhanced protein expression in mammalian cells using engineered SUMO fusions: Secreted phospholipase A(2). *Protein science : a publication of the Protein Society* **17**, 1586-1595

45. Panavas, T., Sanders, C., and Butt, T. (2009) SUMO fusion technology for enhanced protein production in prokaryotic and eukaryotic expression systems. *Methods in molecular biology (Clifton, NJ)* **497**, 303

46. Békés, M., Prudden, J., Srikumar, T., Raught, B., Boddy, M. N., and Salvesen, G. S. (2011) The Dynamics and Mechanism of SUMO Chain Deconjugation by SUMO-specific Proteases. *Journal of Biological Chemistry* **286**, 10238-10247

47. Lian, X., Zhang, J., Azarin, S. M., Zhu, K., Hazeltine, L. B., Bao, X., Hsiao, C., Kamp, T. J., and Palecek, S. P. (2013) Directed cardiomyocyte differentiation from human pluripotent stem cells by modulating Wnt/beta-catenin signaling under fully defined conditions. *Nature protocols* **8**, 162-175

16

48. Hosoyama, T., McGivern, J. V., Van Dyke, J. M., Ebert, A. D., and Suzuki, M. (2014) Derivation of Myogenic Progenitors Directly From Human Pluripotent Stem Cells Using a Sphere-Based Culture. *Stem cells translational medicine*

49. Zhang, H., Rajasekaran, N. S., Orosz, A., Xiao, X., Rechsteiner, M., and Benjamin, I. J. (2010) Selective degradation of aggregate-prone CryAB mutants by HSPB1 is mediated by ubiquitin-proteasome pathways. *Journal of molecular and cellular cardiology* **49**, 918-930

17

#The abbreviations used are: sHSP, small molecular weight heat shock protein; HSE, heat shock element; HSF1, heat shock transcription factor 1, ACD, "α-crystallin" domain; DKO, *HSPB5/HSPB2* double knockout mouse; NT-HSPB5, N-terminus of HSPB5; WT, wildtype HSPB5; iPSCs, induced pluripotent stem cells; ZFN, zinc finger nuclease; 343delT/343delT, patient cell line; WT KI/343delT, heterozygous wildtype knock-in control cell line; SSEA-4, stage-specific embryonic antigen 4; OCT-4, octamer-binding protein 4; iSKMs, iPSC-derived skeletal myotubes; iCMs, iPSC-derived cardiomyocytes; TnT, Troponin T; NMD, nonsense-mediate mRNA decay; qRT-PCR, quantitative real-time PCR; *TNNT2*, *Troponin T*; EV, empty vector; s.d., standard deviation; s.e.m., standard error of the mean; Co-IP, coimmunoprecipitation; SUMO, small ubiquitin-related modifier;

FIGURE LEGENDS

FIGURE 1. 343delT iPSC generation and pluripotency characterization. A.) Representative pedigree for the family of the homozygous recessive 343delT patient. Females are represented by circles, males by squares. Filled shapes represent homozygous 343delT. Half-filled shapes represent heterozygous 343delT. B.) Schematic representation of experimental strategy. Dermal fibroblasts derived from the homozygous 343delT patient were reprogrammed into iPSCs (343delT/343delT), with the 343delT mutation indicated by the red star. Heterozygous gene-corrected control iPSCs were generated from the 343delT/343delT iPSCs through gene editing, and have one copy of WT knocked-in to the *HSPB5* locus (WT KI/343delT). WT KI/343delT and 343delT/343delT iPSCs were differentiated to iPSC-derived cardiomyocytes and skeletal myotubes (iCMs and iSKMs, respectively). C.) Direct Sanger sequencing of a PCR product covering the region of interest reveals deletion of the T at position 343 (highlighted in black) in the 343delT/343delT iPSCs. The PCR product from the WT KI/343delT iPSC line was TOPO-cloned into a vector and multiple clones were sequenced. Reads showing WT (top) and 343delT (bottom) were observed, indicating the WT KI/343delT iPSC line is heterozygous for this mutation. WT KI/343delT and 343delT/343delT iPSCs were stained with immunocytochemistry for pluripotency markers D.) nanog (red) and SSEA-4 (green) and E.) OCT-4 (red) and TRA-1-81 (green). Nuclei were counterstained and merged with DAPI (blue). Size bars indicate 50 μm. F.) qRT-PCR was performed on WT KI/343delT and 343delT/343delT iPSCs with the graph depicting mean ± s.e.m. relative expression levels of pluripotency markers *NANOG*, *OCT-4*, *SOX2*, and *TRA-1-60* normalized to *18s rRNA* and compared to human dermal fibroblasts (HDF) derived from the patient. G.) WT KI/343delT and 343delT/343delT iPSCs differentiated to EZ spheres were taken at week 5 of differentiation for qRT-PCR analysis with markers of the three-germ layers: endoderm (*AFP* and *GATA4*), mesoderm (*α-MHC* and *BRACHYURY*), and ectoderm (*β-III-TUBULIN* and *VIMENTIN*). Graph shows mean ± s.e.m. expression values normalized to *18s rRNA* and compared to WT KI/343delT iPSCs. H.) 20 proliferating cells were counted and fully analyzed using G-banding for each cell line with representative karyotype images showing no consistent abnormalities.

FIGURE 2. 343delT protein is not detectable in iSKMs or iCMs though RNA is present. WT KI/343delT and 343delT/343delT iPSCs were differentiated to A.) iCMs or B.) iSKMs and stained with antibodies that recognized NT HSPB5 (red) and troponin T (TnT, green) and merged with DAPI (blue). Size bars

indicate 50 μm. C.) Representative action potentials recorded from spontaneously beating WT KI/343delT (Top) and 343delT/343delT iPSCs (Bottom) cardiomyocytes (n=6). Western blot and qRT-PCR was performed on paired samples derived from WT KI/343delT and 343delT/343delT cells. Western blots of whole cell lysate (WCL) from D.) iCMs and E.) iSKMs probed with antibodies that recognize NT HSPB5 and GAPDH as a loading control. qRT-PCR of F.) iCMs and G.) iSKMs showing mean ± s.e.m. gene expression for *HSPB5* and *TROPONIN T* (*TNNT2*) normalized to *18s rRNA*. Expression is shown as fold change compared with undifferentiated iPSCs.

FIGURE 3. Lack of 343delT protein is not due to degradation, microRNA targeting, or disrupted translation. A.) WT KI/343delT and 343delT/343delT iCMs were treated with DMSO or 10 μM MG132 to inhibit the proteasome for 12 hours. Western blots of WCL were probed with antibodies recognizing NT HSPB5, p21, and GAPDH. Results are representative of two independent experiments. B.) WT KI/343delT and 343delT/343delT iCMs were transfected with scrambled siRNA control (-), or either 40 pmols (+) or 80 pmols (++) siRNA targeting dicer. Samples were harvested 72 hours post-transfection and WCL was run on a western blot and probed with antibodies against NT HSPB5, dicer, c-MYC (N-262), and GAPDH. C.) Equal amounts of pCSC-MYC-WT and pCS2-MYC-343delT plasmids were input into an *in vitro* transcription/translation (TNT) assay along with ^{35}S-labeled methionine/cysteine. Aliquots were taken from reactions at 30 and 90 minutes as indicated and separated by SDS-PAGE, transferred to nitrocellulose membranes and exposed to film (top). Image is representative of 3 independent experiments with quantification (bottom) expressing synthesis over time as arbitrary units indicating band intensity showing mean ± s.d. There is no significant difference in the rate of synthesis over time for WT (21.8 ± 3.4) and 343delT (19.1 ± 6.9) as calculated by student's t-test (p>0.5).

FIGURE 4. 343delT forms visible aggregates when overexpressed and induces a cellular stress response. 343delT/343delT iSKMs were transfected with pCMV-MYC-WT or pCMV-MYC-343delT constructs. Cells were stained 48 hours post-transfection with antibodies recognizing A.) NT HSPB5 (red) and TnT (green) and B.) MYC-tag (green) and desmin (red). Size bars indicates 25 μm. BHK21 cells were transfected with pCMV-MYC-WT or pCMV-MYC-343delT constructs for 24 hours and co-stained with antibodies against C.) NT HSPB5 (red) and MYC tag (green), D.) MYC-tag (green) and desmin (red), and E.) MYC-tag (green) and HSP70 (red). Size bars indicate 50 μm. In all merged immunocytochemistry images, nuclei were counterstained and merged with DAPI (blue). Enlargements of the area within the white dotted box are shown at the right. Arrows indicate 343delT aggregates. F.) WCL from BHK21 cells transfected as above or similarly with pCMV-MYC-empty vector (EV) were analyzed by western blot with antibodies recognizing HSP70, MYC (9E10), and α-tubulin as a loading control. Samples were run in duplicate.

FIGURE 5. WT co-expression reduces 343delT aggregates and increases solubility of the mutant protein. A.) BHK21 cells were transfected with pCMV-HA-WT, pCMV-MYC-343delT, or both (co-transfection) and stained with antibodies against HA-tag and MYC-tag after 24 hours. Nuclei were counterstained and merged with DAPI (blue). Enlargements of the area within the white dotted box are shown at the right. Arrows indicate 343delT aggregates. Size bar indicates 50 μm. B.) BHK21 cells were transfected with pCMV-HA-WT, pCMV-HA-WT and pCMV-MYC-343delT (co-transfection), pCMV-MYC-343delT, or pCMV-MYC-WT, harvested 24 hours post-transfection, and fractionated into soluble and insoluble fractions or whole cell lysate (WCL). Equal amounts of protein were loaded for western blot using an anti-MYC (9E10) antibody and an HA-tag antibody with β-actin as a loading control. Image depicts representative blots from 3 independent experiments. C.) The percentage of insoluble 343delT, quantified using the 15 kDa-sized band ([insoluble] $_{density}$ *100 / ([insoluble] $_{density}$ + [soluble] $_{density}$)) is shown in the bar graph. Insoluble 343delT is reduced 6.6 fold by co-expression with WT (343delT alone = 99 ± 1% insoluble 343delT, 343delT + WT = 15 ± 6% insoluble 343delT, mean ± s.d., n=3, p-value of <0.01 as calculated by student's t-test). D.) BHK21 cells transfected as in (B) were harvested after 24 hours for Co-IP using RIPA buffer and immunoblotted with anti-HA-tag or anti-MYC (9E10) antibodies. Western

19

blots were performed showing IP fractions as well as WCL and the insoluble fraction (remaining pellet from sample solubilized in RIPA buffer) and stained with antibodies against MYC (9E10), HA-tag and α-tubulin as a loading control.

FIGURE 6. *In vitro* refolding of 343delT in the presence of WT and SUMOylation in cells rescue 343delT insolubility. A.) Recombinant 343delT expressed in *E.coli* was found to accumulate within insoluble inclusion bodies (I) and not within the soluble lysate (S). B.) Refolding WT or a 343delT:WT mixture resulted in a soluble product that was not removed upon passing through a 0.22 µm filtration device. Refolding of 343delT in the absence of WT resulted in aggregates that were removed from solution upon filtration. U= unfiltered, F= filtered. C.) 300 µL of refolded WT and refolded 343delT:WT mixture from (B) were loaded in subsequent runs onto a Superdex 200 10/300 column (pre-equilibrated into 200 mM ammonium acetate pH 6.9). Separation was carried out at a flow rate of 0.4 mL/minute and absorbance monitored at 280 nm. The chromatogram for the 343delT:WT mixture (orange) had a slight shoulder and was shifted to earlier elution volumes compared to WT alone (purple). 9 µL of fractions 9-17 were analyzed by SDS-PAGE for each run, alongside molecular weight markers. These revealed the co-elution of 343delT with WT. D.) Corresponding fractions from each run in (C) were analyzed by means of native mass spectrometry. The control containing WT displayed a complicated overlapping signal centered near 10,000 *m/z*, relating to multiple charge state series of WT oligomers. For the mixture, two areas of interest were identified, a region around 10,000 *m/z* akin to the WT spectra and a charge state series at 2,000 *m/z*. This was identified to correspond to monomeric 343delT (Mw = 14,695 Da). Close inspection of the region at high m/z (inset), reveals peaks in the 343delT:WT mixture that cannot arise from WT homo-oligomers, but rather correspond to an ensemble of hetero-oligomers comprising both HSPB5 components. E.) BHK21 cells were transfected with pCMV-MYC-WT, pCMV-MYC-SUMO3 Q89P-WT, pCMV-MYC-343delT, or pCMV-MYC-SUMO3 Q89P-343delT, harvested 24 hours post-transfection, and WCL was isolated. Equal amounts of protein were loaded for western blot using an anti-MYC (9E10) antibody with β-actin as a loading control. Image depicts a representative blot from 3 independent experiments with longer exposure shown at the right. Relative increase in WT and 343delT proteins with the addition of SUMO is indicated below the respective lanes. WT increased 6 ± 1 fold, while 343delT increased 130 ± 60 fold (mean ± s.d. of 3 independent experiments) with a p-value of <0.05% as calculated by student's t-test. F.) 343delT/343delT iCMs were transfected with pCMV-MYC-343delT or pCMV-MYC-SUMO3 Q89P-343delT and harvested 24 hours post-transfection. Analysis of WCL by western blot was performed using an anti-MYC (9E10) antibody with β-actin as a loading control with longer exposure shown at the right. Relative increase in 343delT protein with the addition of SUMO is indicated (811 ± 218 fold) as mean ± s.d. of 3 independent experiments.
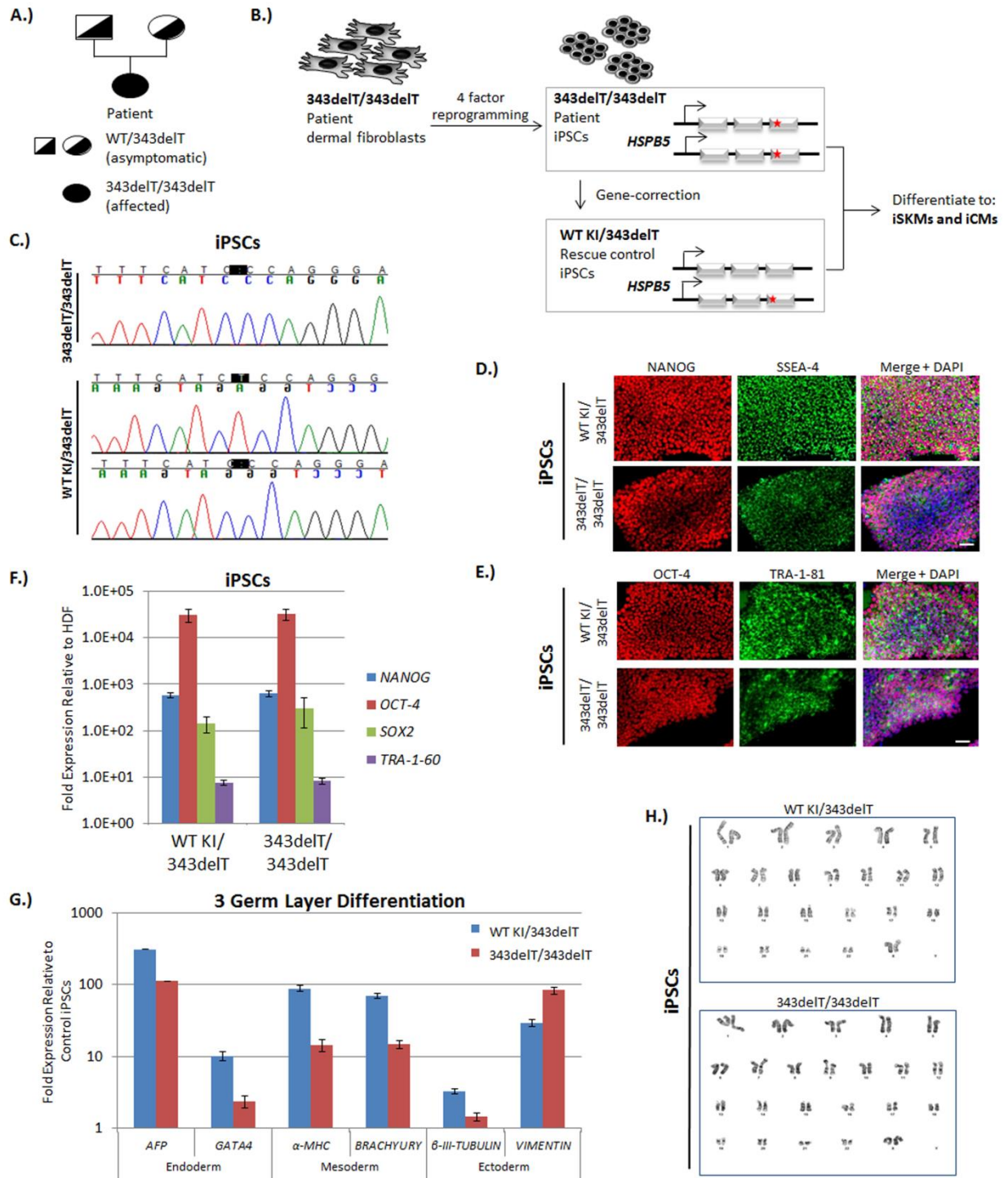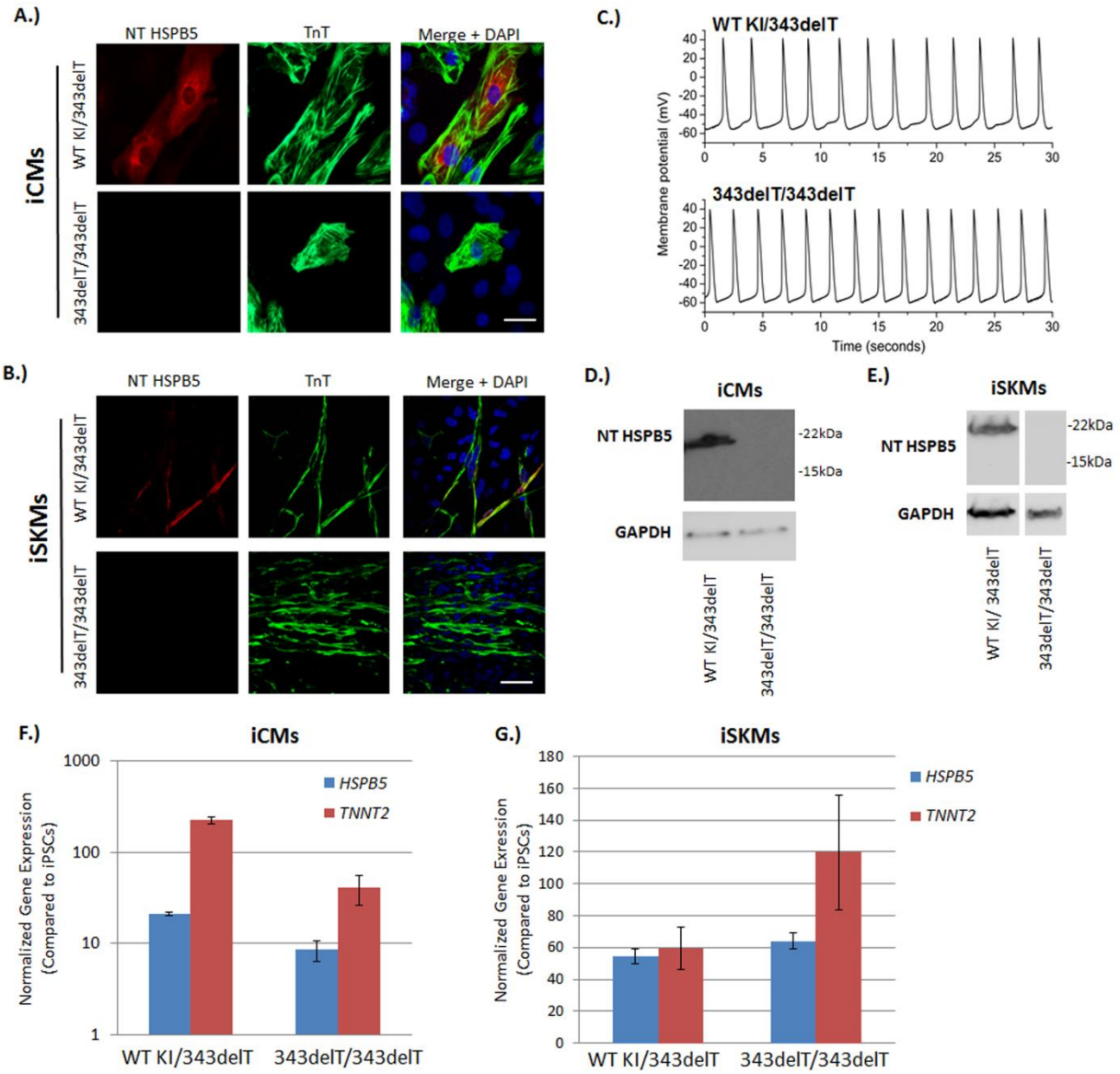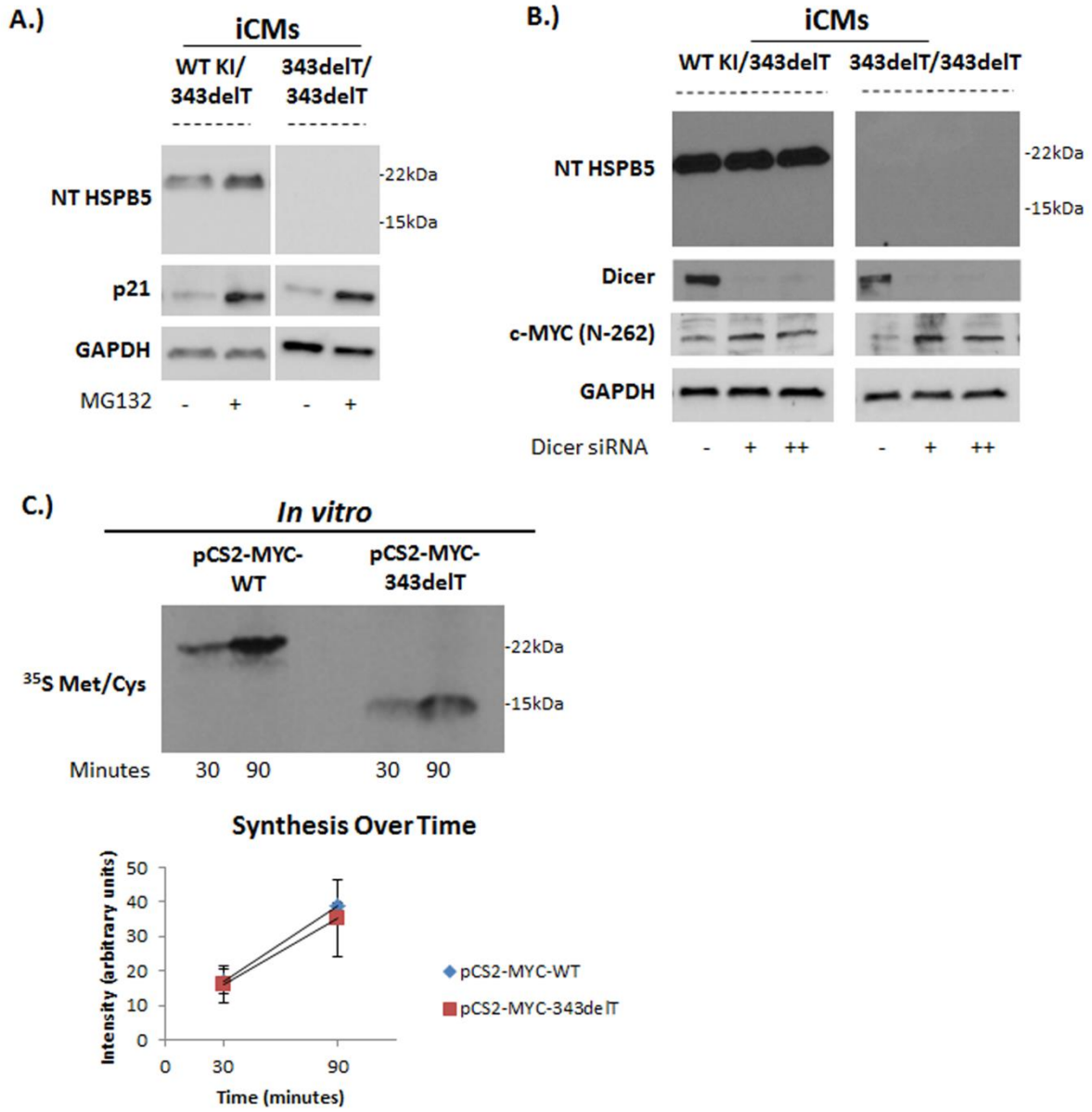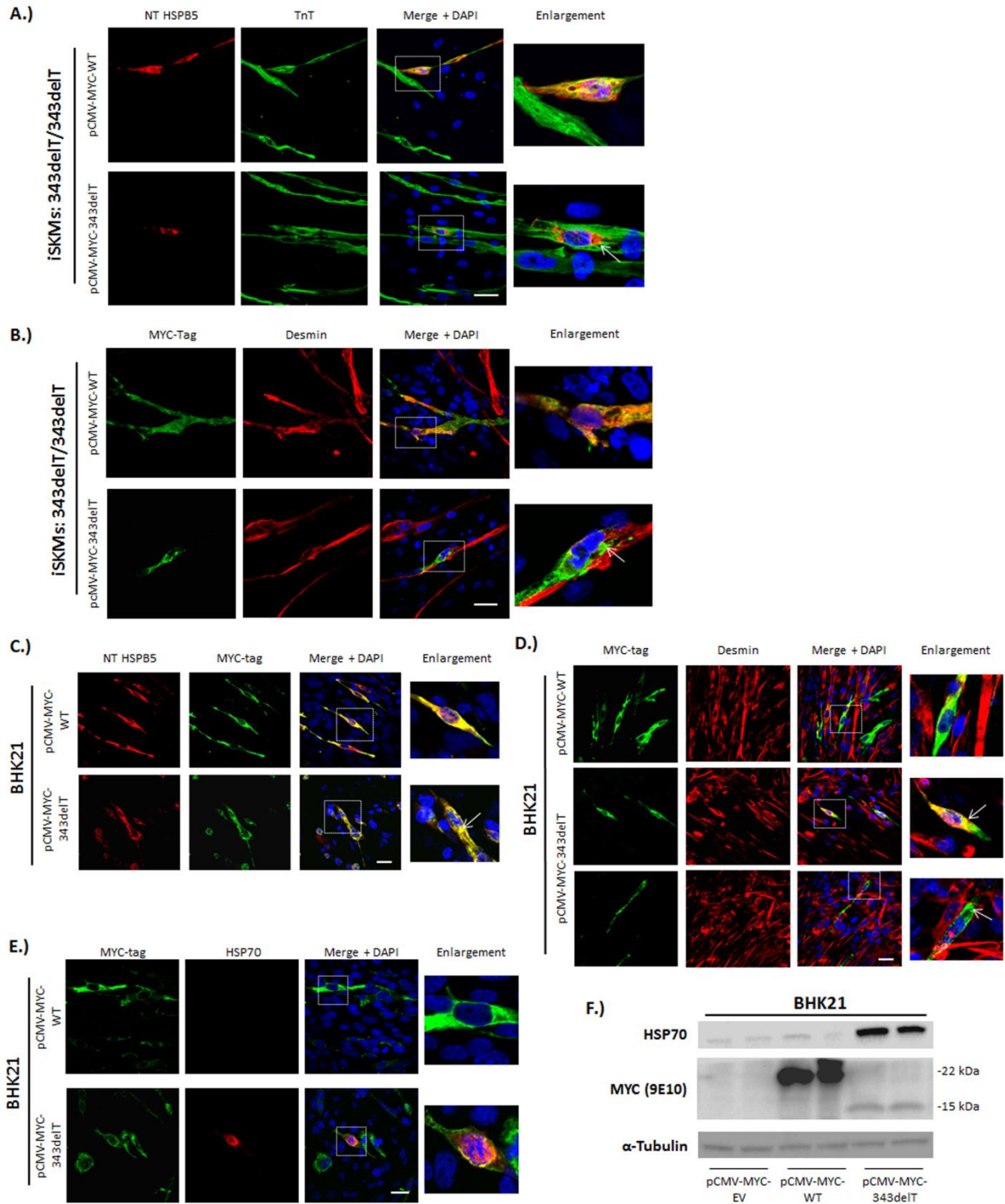
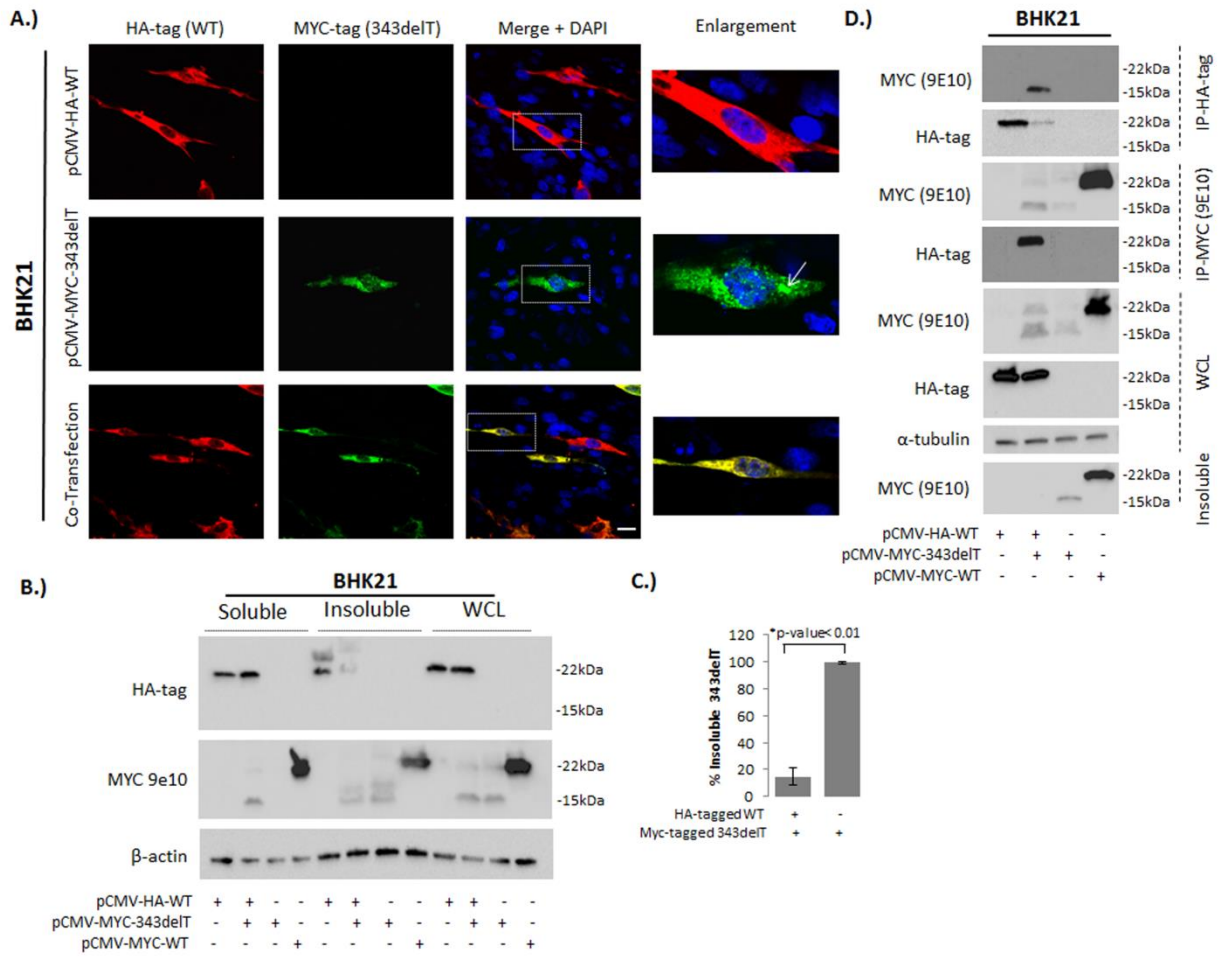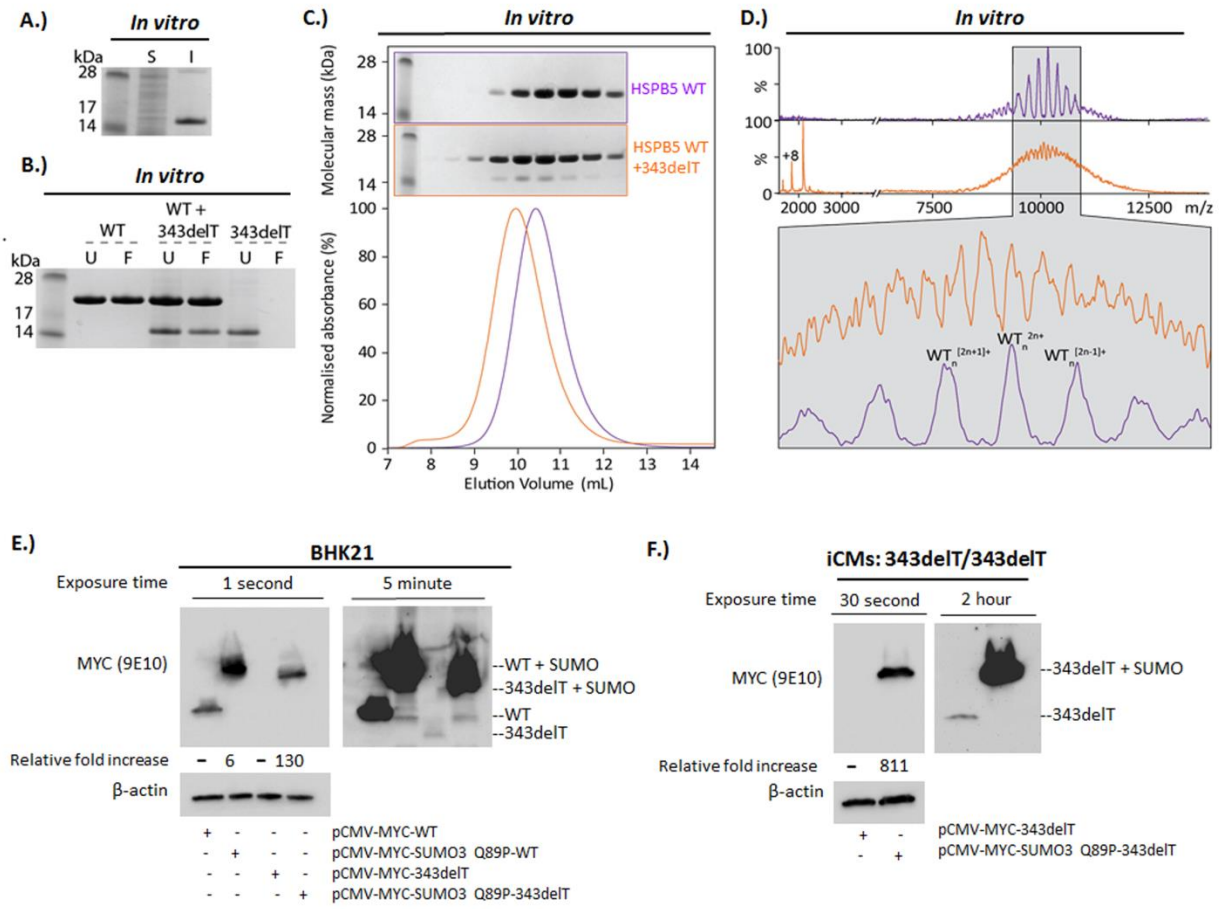Figure 1

Figure 2

Figure 3

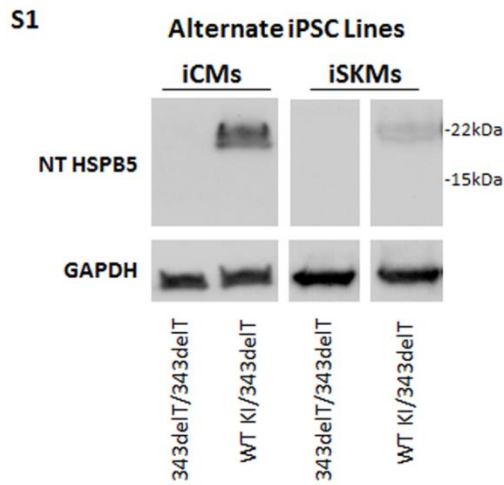Figure 4

24

Figure 5

Figure 6

Human 343delT HSPB5 Chaperone associated with Early-onset Skeletal Myopathy causes Defects in Protein Solubility

Katie A. Mitzelfelt, Pattraranee Limphong, Melinda J. Choi, Frances D.L. Konrat, Shuping Lai, Kurt D. Kolander, Wai-Meng Kwok, Qiang Dai, Michael N. Grzybowski, Huali Zhang, Graydon M. Taylor, Qiang Lui, Mai T. Thao, Judith A. Hudson, Rita Barresi, Kate Bushby, Heinz Jungbluth, Elizabeth Wraige, Aron M. Geurts, Justin L.P. Benesch, Michael Riedel, Elisabeth S. Christians, Alex C. Minella, Ivor J. Benjamin

SUPPLEMENTARY DATA

Supplementary Figure S1: Lack of 343delT Protein in an Alternate iPSC Line
An alternate iPSC line derived from 343delT/343delT patient dermal fibroblasts was gene-corrected using the same approach as described previously. Both lines were differentiated to iCMs and iSKMs and a western blot was performed and probed with antibodies that recognize NT HSPB5 and GAPDH as a loading control.

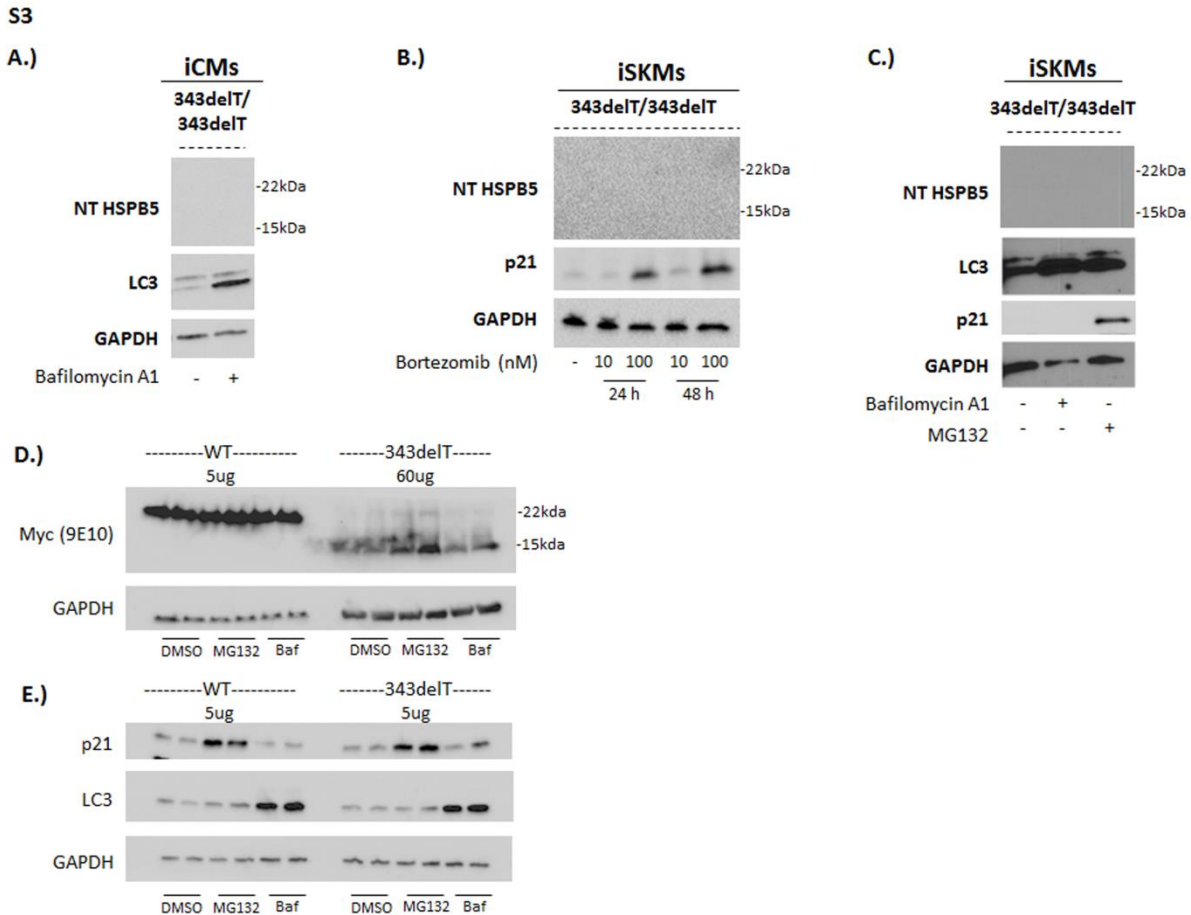**Supplementary Figure S2: 343delT Transcript Stability**
To measure *HSPB5* transcript stability, iCMs were re-plated on day 27 as described in Experimental Procedures and seeded into a 12 well 0.1% gelatin coated plate at 80% confluency. The following day, cells were treated with 1μM actinomycin D (Sigma) to inhibit transcription and harvested at indicated time points for qRT-PCR. *HSPB5* mRNA and *MYC* (an unstable control mRNA) levels were normalized to *18s rRNA* and plotted as mean ± s.e.m. expression relative to 0 hour WT KI/343delT sample. Data is representative of two independent experiments performed. Decrease in *MYC* transcript levels from 0-4 hours indicates the actinomycin D treatment successfully inhibited transcription. *HSPB5* levels did not decline over 24 hours, indicating transcript stability. The unexpected increase in *HSPB5* mRNA levels may be explained by incomplete inhibition of transcription by actinomycin D, which acts as a cellular stress and upregulates stress response genes including *HSPB5*.
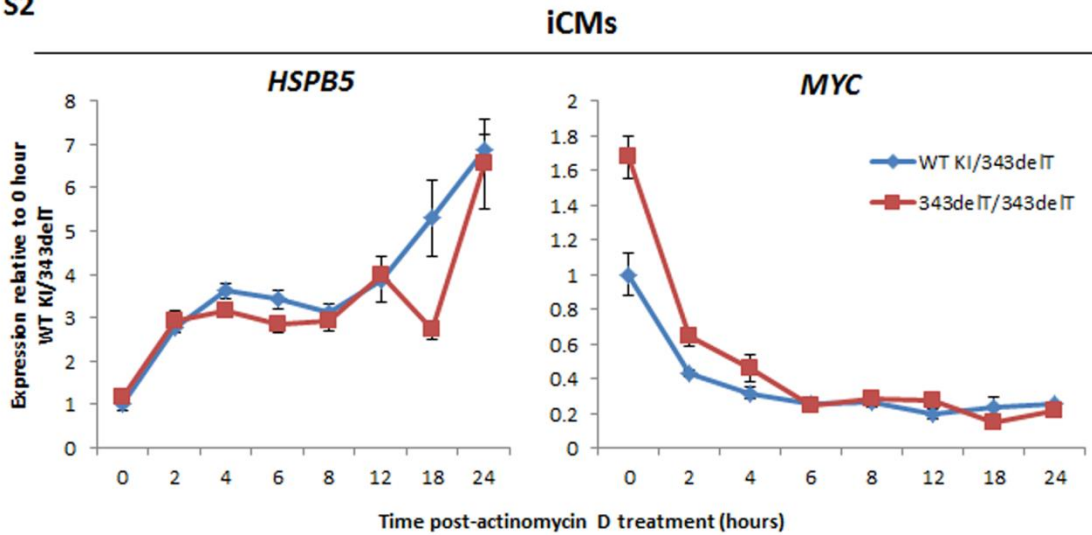
Supplementary Figure S3: Overexpressed 343delT Protein is Degraded by Both the Proteasome and Autophagy

A.) 343delT/343delT iCMs were treated with DMSO or 80 nM bafilomycin A1 to inhibit autophagy for 12 hours. Western blots of WCL were probed with antibodies recognizing NT HSPB5, LC3, and GAPDH. Results are representative of two independent experiments. B.) 343delT/343delT iSKMs were treated with DMSO (-) or 10 or 100nM bortezomib for 24 or 48 hours to inhibit the proteasome and WCLs were probed by western blot with antibodies recognizing NT HSPB5, p21, and GAPDH. C.) 343delT/343delT iSKMs were treated with DMSO (-), 80nM bafilomycin A1, or 10μM MG132 for 12 hours and WCL were run on western blots probed with antibodies recognizing NT HSPB5, LC3, p21, and GAPDH. MCF7 cells were transfected with pCMV-MYC-WT or 343delT constructs for 24 hours followed by treatment with DMSO, 5 μM MG132, or 80 nM bafilomycin (Baf) for 12 hours. D.) Western blots with 5 μg (WT) or 60 μg (343delT) of WCL were stained with antibodies against MYC (9E10) and GAPDH as a loading control. Samples are shown in duplicates. Results are representative of two independent experiments. E.) 5 μg of protein for each of the same samples in (D) was run on a gel and stained with antibodies against p21, LC3, and GAPDH. Both inhibition of the proteasome (MG132) and inhibition of autophagosome maturation (Baf) resulted in slightly elevated levels of 343delT.

Supplementary Figure S4: Transfection and RNA levels are Equal between WT and 343delT
A.) MCF7 cells transfected with pCMV-MYC-WT or 343delT HSPB5 constructs were harvested 2, 4, 6, or 24 hour after transfection for qRT-PCR. Graph shows mean ± s.e.m. ΔCt values for *HSPB5* normalized to *18s rRNA* from n=3. B.) MCF7 cells were transfected with empty vector (EV) (1 μg) or pCMV-MYC-WT in increasing amounts (0.01 μg, 0.1 μg, 1 μg). Samples (n=4 for each group) were harvested 24 hours after transfection and divided using half for qRT-PCR analysis of gene expression (left graph) and the other half fixed and analyzed by flow cytometry (right graph). *HSPB5* gene expression is normalized to *18s rRNA*, with the graph expressing mean ± s.e.m. fold change relative to EV. Transfection efficiency was analyzed by flow cytometry using anti-MYC-tag (Cell Signaling 2278, 1:500) with the graph showing mean ± s.d. percentage of MYC-tag positive cells. Results indicate similar transfection efficiencies between WT and 343delT.
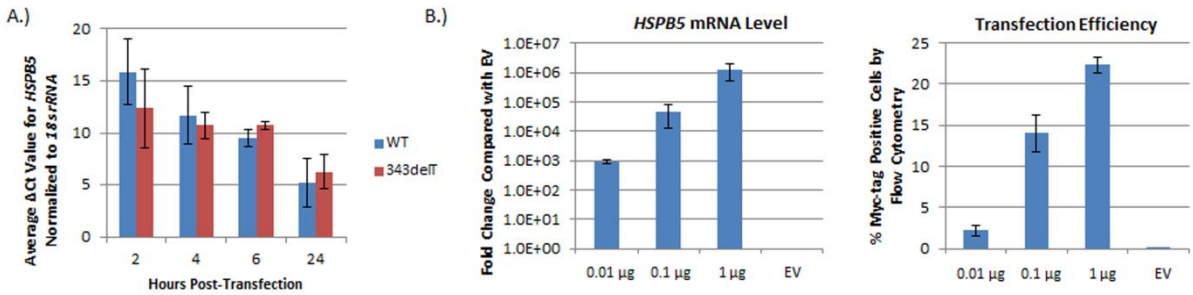
Supplementary Figure S5: Effects of 343delT Expression on Proliferation and Cell Toxicity
HEK 293FT cells transfected with EV, myc-tagged WT, or myc-tagged 343delT were harvested after 24 hours and A.) total cell number as well as B.) percent viable cells by trypan blue staining were counted using a Countess Automated Cell Counter (Life Technologies). Graphs depict mean ± s.d. from n=4 for each group. Results indicate no impact on cell proliferation or viability with transfection of WT or 343delT constructs.
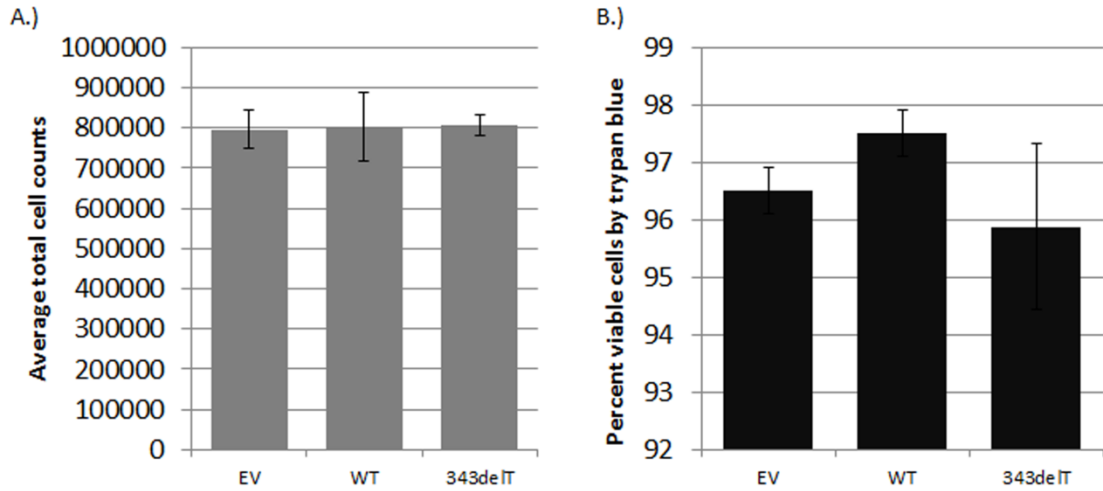
Human 343delT HSPB5 Chaperone associated with Early-onset Skeletal Myopathy causes Defects in Protein Solubility

Katie A. Mitzelfelt, Pattraranee Limphong, Melinda J. Choi, Frances D. L. Kondrat, Shuping Lai, Kurt D. Kolander, Wai-Meng Kwok, Qiang Dai, Michael N. Grzybowski, Huali Zhang, Graydon M. Taylor, Qiang Lui, Mai T. Thao, Judith A. Hudson, Rita Barresi, Kate Bushby, Heinz Jungbluth, Elizabeth Wraige, Aron M. Geurts, Justin L. P. Benesch, Michael Riedel, Elisabeth S. Christians, Alex C. Minella and Ivor J. Benjamin